65

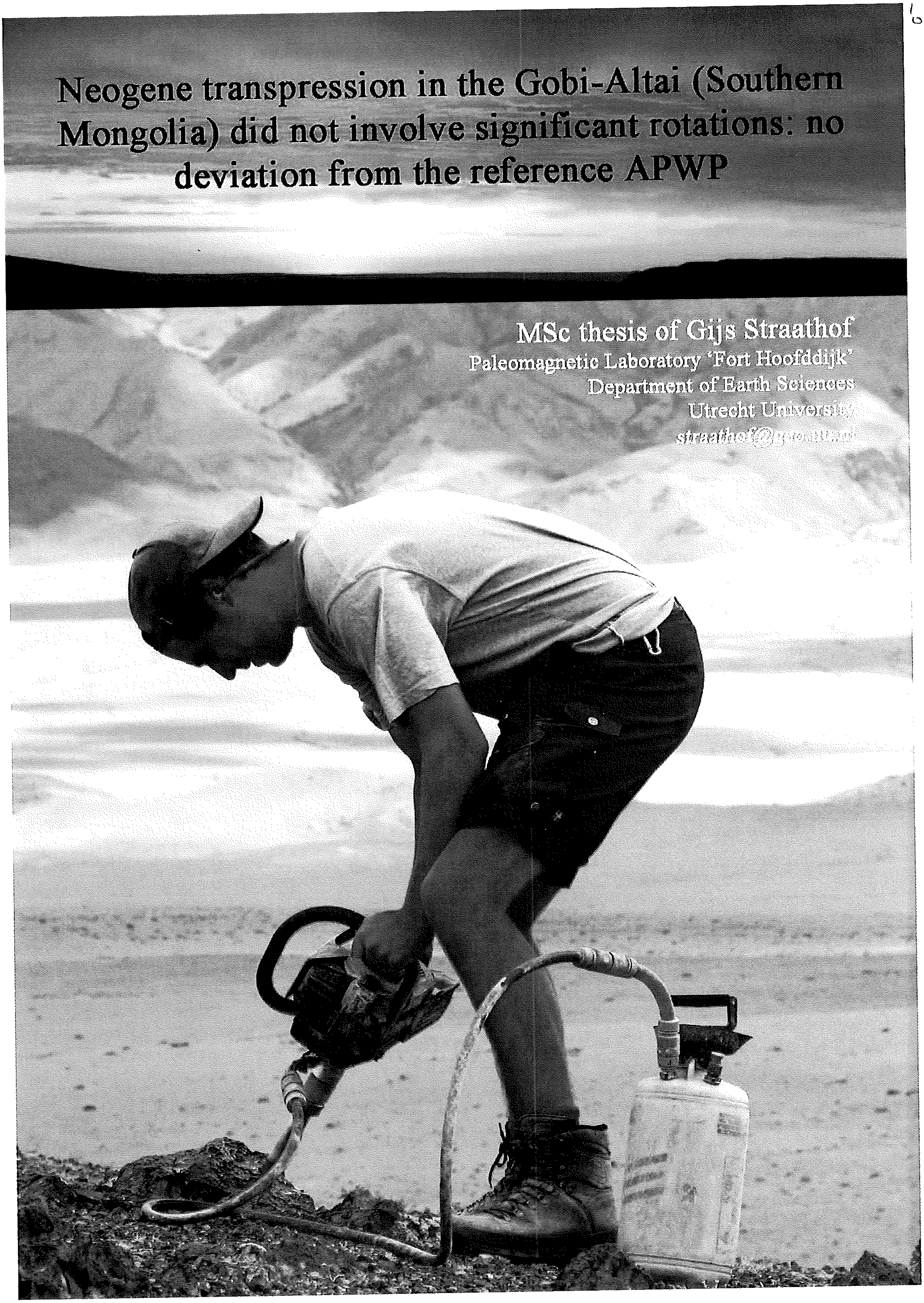

Neogene transpression in the Gobi-Altai (Southern Mongolia) did not involve significant rotations: no deviation from the reference APWP

MSc thesis of Gijs Straathof
Paleomagnetic Laboratory 'Fort Hoofddijk'
Department of Earth Sciences
Utrecht University
straathof@geo.uu.nl

Contents

Neogene transpression in the Gobi-Altai (Southern Mongolia) did not involve significant rotations: no deviation from the reference APWP

Gijs Straathof

Paleomagnetic Laboratory 'Fort Hoofddijk', Utrecht University
Orogenic Processes Group, University of Leicester
straathof@geo.uu.nl

Abstract

A paleomagnetic study has been carried out to discriminate between two end-member scenarios on the intra-continental, transpressional strike-slip system in the Gobi-Altai, southern Mongolia. The first suggests that these strike-slip faults utilise obliquely oriented weak Paleozoic or Mesozoic zones in the basement. The second scenario suggests that initial strike-slip faults become transpressional as a result of vertical axis rotations, caused by increased shortening from east to west. We sampled lower Cretaceous basalts, and some younger lavas and basalt plugs. Approximately 1040 samples were drilled in 17 localities in lower Cretaceous and Cenozoic lavas, each subdivided into 4-15 sites of 7 samples each. These were then demagnetised using alternating field (AF) and thermal demagnetisation techniques. Rock magnetic analysis includes determination of Curie temperatures (560- 580°C) and indicates magnetite as the main carrier of the magnetic signal. Three positive foldtests give us confidence that our high temperature-component is the primary magnetisation. The results show a mean direction of declination/inclination (D/I) = 12.3/66.5 (a95=2.3; k=43.4), which does not statistically deviate from the published average Eurasian paleomagnetic direction for this time window (D/I = 13.6/63.0; a95 = 1.7, from Besse and Courtillot, 2002). We thus conclude that Neogene transpressional mountain building in the Gobi Altai of southern Mongolia was not associated with rotation of strike-slip faults. Moreover, we show that southern Mongolia has belonged to the Eurasian continent since at least the early Cretaceous.

Introduction

Active intracontinental strike-slip deformation is often associated with transpression and is one of the major mountain building processes. Examples are formed by the Chaman & Ornach-Nal faults in the Middle East (Vernant et al., 2004), the northern South Island of New Zealand (Collot et al., 1996), the Coastal Cordillera Fault Zone in Chile (Taylor et al., 1998), the San Andreas fault system in western North America (Wesnousky, 2005) and the Western Altai and Gobi-Altai in Central Asia (Tapponnier and Molnar, 1979; Cunningham, 2005). The concept of discrete block rotations within a distributed fault system is commonly applied to most intracontinental strike-slip settings. Garfunkel (1988) and Nur et al. (1988) proposed a rigid block rotational model where rotations are explained in association with strike-slip movement along major fault zones.

This study concerns the vertical axis rotations associated with transpressional mountain building in the Gobi-Altia, Central Asia (Figure 1). Following the closure of the last intra-Asian "Mongol-Okhotsk" ocean, in the late Jurassic (Tapponnier and Molnar, 1979; Zhao et al., 1990; Enkin et al., 1992; Cogne et al., 2005), the Cenozoic India-Asia collision led to the formation of intracontinental deformation in Central Asia (Tapponnier and Molnar, 1979). The stress-field derived from the collision extends progressively through Tibet and the Tien Shan into southern Mongolia where transpressional strike-slip faults comprise far-field deformational response to the

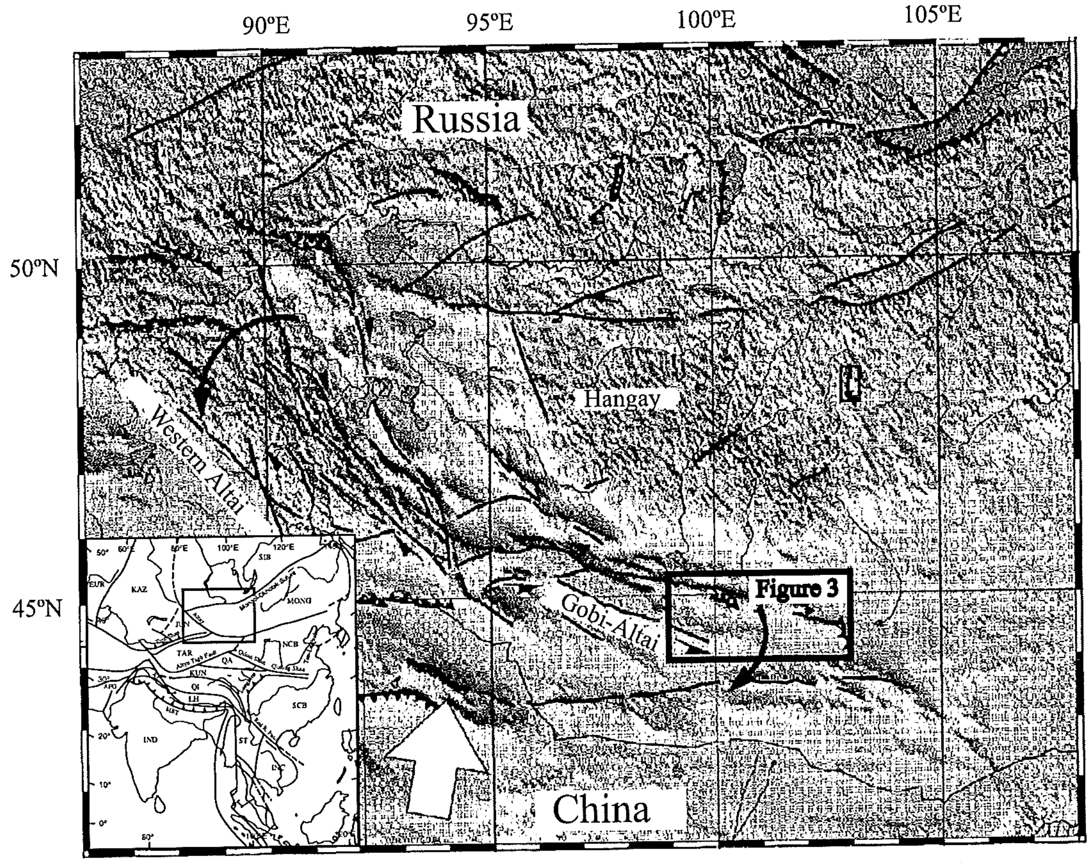

Figure 1: Topographic map of Western Altai and Gobi-Altai. Big white arrow indicates the direction of maximum stress, the dark arrows indicate the sence off rotation according to the model of Schlupp (1996); obtained from Baasgalan, 1999).

collision (Cunningham et al., 1996; Cunningham, 2005). The NNE directed maximum stress meets the Hangay Dome, a Precambrian rigid block in central Mongolia, which directs deformation west and south of the craton forming the Western Altai and the Gobi-Altai mountain ranges respectivily (Cunningham, 1998, 2005). To achieve shortening in the direction of maximum stress, Schlupp (1996) suggested a rotational model in which the Western Altai rotate counterclockwise and the Gobi-Altai rotate clockwise. In this way, both ranges rotate towards a direction more orthogonal to the direction of maximum stress (Figure1).

The Gobi-Altai fault system, also called Bogd Fault, is a left-lateral, E-W trending strike-slip fault system with restraining bends forming the highest mountain ranges (Cunningham et al., 1996). Different scenarios explain the origin of the transpressional strike-slip in this system, including those which suggest that pre-existing weakness zones, related to e.g. Mesozoic extension or Paleozoic terrane accretion reactivated as oblique strike-slip faults (Cunningham, 1998), and others that make use of vertical axis rotations causing strike-slip faults to become transpressional (Bayasgalan and Jackson, 1999).

The aim of this study is to provide constraints on the model for generation of transpressional strike-slip deformation in the Gobi-Altai. This will be done by analysing paleomagnetic data from Gobi-Altai volcanic rocks which are collected on both sides of the faults to detect rotation differences. From the obtained paleomagnetic directions an apparent polar wander path (APWP) will be created and compared to the reference APWP of Eurasia. Results of previous studies reveal a rigid behaviour of Mongolia with respect to Eurasia since the early Cretaceous e.g. (Zonenshain et al., 1990; Enkin et al., 1992). Any discrepancy of the polar wander path would thus imply local deformation in the Bogd Fault. We interpret any present rotations in terms of the proposed mechanisms for restraining bend formation and strike-slip fault connectivity.

The Gobi Altai fault system is very suitable for a paleomagnetic study of this purpose because its structure is well known (Cunningham et al., 1996) and the stratigraphy in boundary basins contains well exposed, extensive lavas and shallow intrusives of Cretaceous to Neogene age (Traynor and Sladen, 1995; Barry, 1999). Figure 2 summarises the configuration of Asian blocks during the Mesozoic, after Enkin et al.

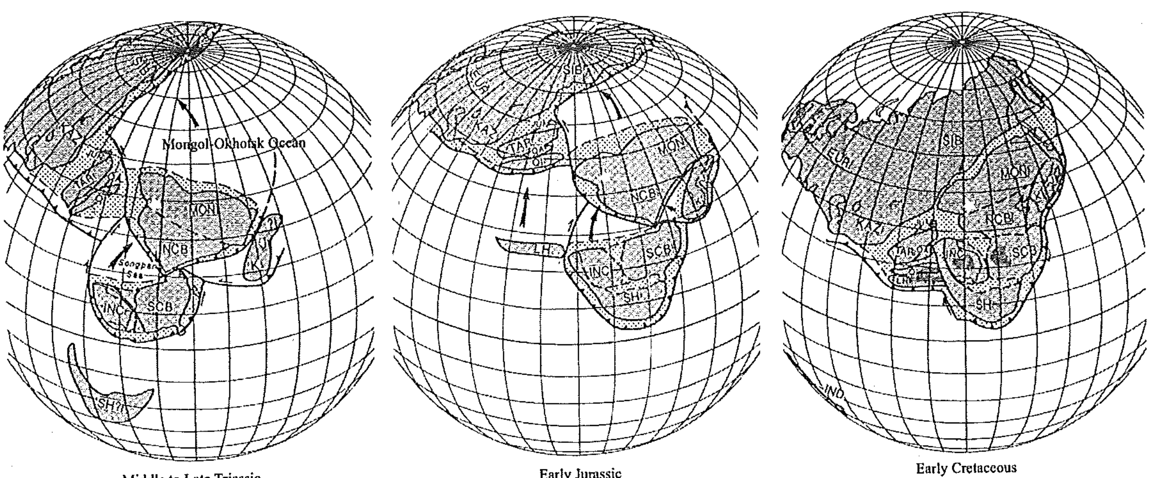

Figure 2: Mesozoic reconstruction of Asian blocks of Enkin et al. (1992). The Early Cretaceous configuration shows the final configuration before the India-Eurasia collision started in the Cenozoic. The Mongolia block (MON) and the North China Block (NCB) followed the same path during the Mesozoic. The Mongol-Okhotsk suture zone is located between the Mongolia block and Siberia. White star indicates the study site.

(1992). After the Mongolian tectonic unit joined the North China Block in the Permian (Zhao et al., 1990; Enkin et al., 1992; Pruner, 1992) they amalgamated with Eurasia. Studies in the Mongol-Okhotsk Suture belt have shown that the closure of the Mongol-Okhotsk ocean was finished in the early Cretaceous (Cogné et al., 2005), although the exact timing is still under debate (Zhao et al., 1990; Enkin et al., 1992; Cogné et al., 2005). Because the position of Mongolia appears to have been relatively stable since the mid Mesozoic, early Cretaceous deposits are suitable to study recent deformational features.

Regional Geological Setting

The Asian continent consists of an assemblage of accreted terranes that amalgamated during Pre-Mesozoic times (Sengör et al., 1993). The terrane distribution of Mongolia is defined in more detail by Badarch et al. (2002) and Helo et al. (2006). The accretion of Paleozoic terranes has led to a well defined structural grain around the Hangay region (Cunningham, 1998, Figure 2), which in the Gobi-Altai region has a WNW-ESE trend.

A period of crustal extension started in the Mid-Jurassic and continued during the Cretaceous, leading to the formation of a belt of Mesozoic basins throughout Mongolia (Traynor and Sladen, 1995). The basins are organised along an E-W general trend, subparallel to the Paleozoic structural grain. The sedimentary sequences within the basins are characterised by syn-rift, continental deposits unconformable on the basement. The stratigraphy shows lithological variations from basin to basin, but generally, syn-rift volcanic rocks alternate with alluvial and fluvial clastic sediments or lacustrine mudstones (Traynor and Sladen, 1995; Johnson et al., 2001; Howard et al., 2006).

During the mid Cretaceous, the southern Mongolian basins experienced uplift caused by transpression and thrusting. Widespread post-rift alluvial and fluvial sedimentation occurred from the late Cretaceous onwards during which the topography was reduced. This left the Gobi-Altai with erosional surfaces and thin sedimentary sequences (Traynor and Sladen, 1995).

The stressfield induced by the India-Eurasia collision led to northward propagating deformation (Tapponnier and Molnar, 1979). This resulted in transpressional mountain building in two zones around the Hangay Dome (Cunningham, 1998, 2005), in the Western Altai since the Oligocene and in the Gobi-Altai since the late Miocene (Howard et al., 2003; Vassallo et al., 2006). The tops of the current mountain ranges are formed by the erosional surfaces of the upper and post Cretaceous (Berkey and Morris, 1927; Devyatkin and Smelov, 1980). The basins in between contain upper Cretaceous and Tertiary sediments flanking and unconformably overlying the Paleozoic basement and deformed Jurassic-lower Cretaceous basin fill within and adjacent to the restraining bend mountains (Cunningham et al., 1996).

Structure and Stratigraphy of the Gobi-Altai

Cenozoic deformation in southern Mongolia caused right-lateral transpressional strike-slip deformation in the Western Altai and left-lateral transpression in the Gobi-Altai (Cunningham, 1998, 2005). The studied area comprises the transpressional mountain ranges of Ih Bogd, Baga Bogd and Artz Bogd in the eastern Gobi-Altai, southern Mongolia (100°–102°E, 44°–45°N, Figure 1) which is characterised by east-west trending, left-lateral strike-slip segments. These segments are connected by restraining bends with elevations upto ±1500 m with respect to the surrounding basins (Cunningham et al., 1996; Cunningham et al., 1997). The restraining bends developed progressively eastward with time, creating flower structures (Cunningham et al., 1996), and the driving faults are still active, as revealed by recent seismic activity (Baljinnyam

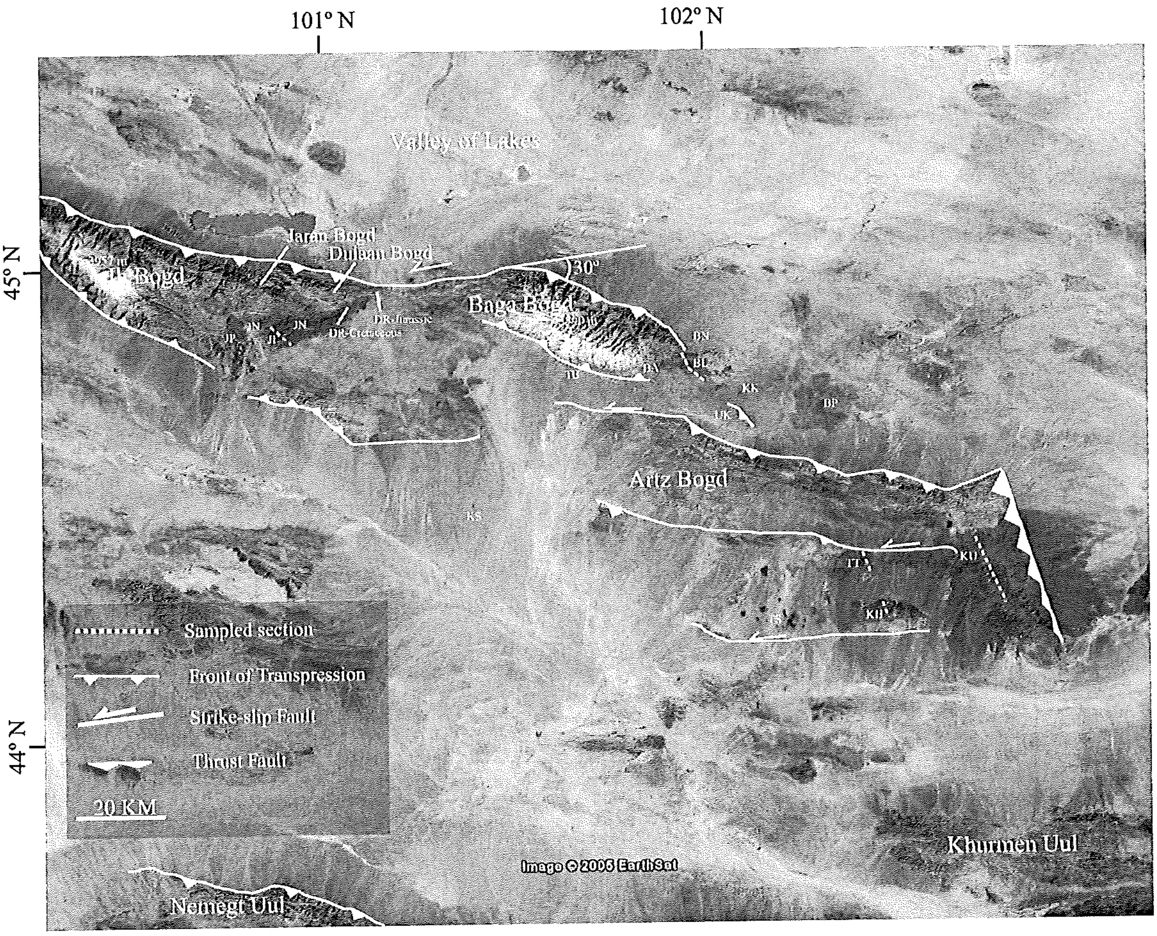

Figure 3: EarthSat Image of the fieldwork area showing the geographical distribution of the sampling localities. The main faults are indicated. Sample codes according to Table 1.

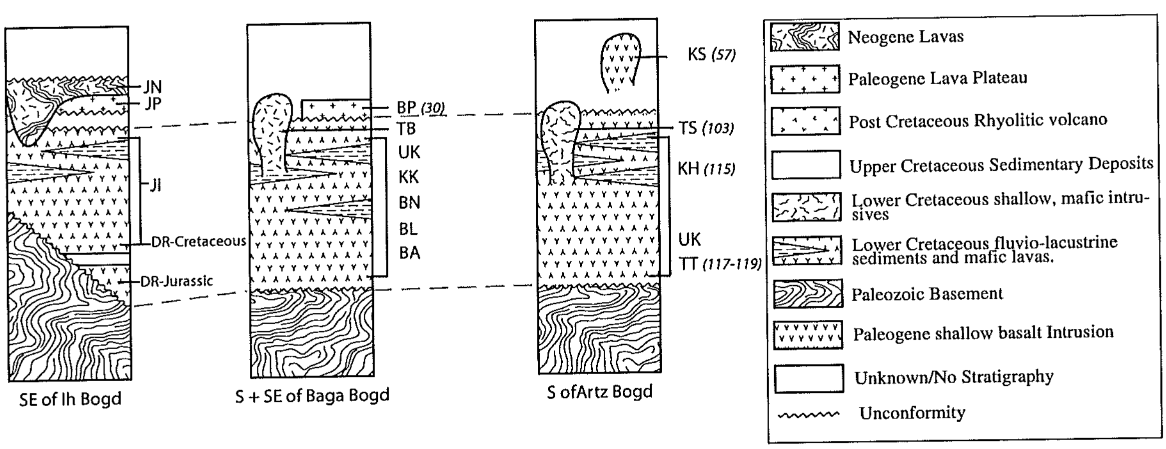

Figure 4: Stratigraphic columns for three restraining bend border belts in the field area. The localities show their relative stratigraphic position. Known ages are indicated (Ma). Sample codes according to Table 1.

Locality	N-sites	age	ref	Field relations	remarks
Dulaan Bogd (DR) Jurassic	10	*JU*	Field Relations	Steeply dipping, folded lavas.	
Jaran Bogd (JI)	27	*110-90 Ma*	Field Relations	Continuous stratigraphy of alternating lavas and mudrocks, south dipping with a monocline folding the top flows.	The base of the section is close to the Jaran Bogd volcano. At the top, the stratigraphy is unconformably overlain by sediments of late and post Cretaceous times.
Dulaan Bogd (DR) Cretaceous	7	*110 Ma*	Field Relations	Continuous stratigraphy of lavas interbedded by red, clastic sediments.	Lateral equivalent of the lower part of the Jaran Bogd stratigraphy.
Jaran Plateau (JP)	10	*30 Ma*	Field Relations	Elevated, subhorizontal volcanic plateau.	Sites are spread out over the plateau. The entire locality might be build up out of one lava.
Jaran Bogd Neogene (JN)	7	*5 Ma*	Field Relations	Lavas filling the topography eroded into the Cretaceous section.	Three lavas were sampled at 7 sites in total. The lavas orginate from the Jaran Bogd volcano.
Baga Bogd (BA)	7	*130 Ma*	Russian map	Continuous sequences of lavas on the southern flanks of Baga Bogd	Sampling took place in a dry river bed.
Bulgantiin Uul (BL)	15	*130 Ma*	Russian map	Section of successive lava flows. After the first 10, the lavas are interbedded by sand-clay deposits.	Lateral equivalent of BA. Sampling took place in a dry river bed.
Baga Bogd North (BN)	7	EC	Field Relations	Steeply dipping lavas sticking out of recent sedimentary deposits creating lense-shaped outcrops.	North of Baga Bogd. Probably laterally equivalent to BL.
Khalzan Khairkhan (KK)	7	EC	Field Relations	A topographic high formed by a stack of lavas, subhorizontally overlying sediments.	This locality probably forms the top of the BL section, but the section is not continuous due to little exposure in between.
Unegt Khairkhan (UK)	7	EC	Field Relations	Steeply dipping lavas forming a ridge-like morphology.	The tilt is a consequence of thrusting in the area between Baga Bogd and Artz Bogd.
Bogd Plateau (BP)	14	30.46±0.09 Ma	(Barry, 1999)	Elevated, subhorizontal volcanic plateau, consisting of a northern and a southern part split by a fault.	7 sites were collected on each side of the fault, equally spread around the plateau. This locality might consist of a few lavas only.
Tsagaanbotga (TB)	4	PC	Field Relations	Rhyolitic plug on the southern flank of Baga Bogd.	No bedding identified. Only 4 sites, due to the poor quality of the outcrops.
Tsagaan Tsav (TT)	10	117.4-119.3±0.36 Ma	(Barry, 1999)	Continuous series of south-east dipping lavas.	Sampling took place in a dry river bed.
Kharaat Uul (KU)	10	*120 Ma*	Field Relations	Long stratigraphy of southdipping lavas crosscut by a horsetail splay halfway the section.	Lateral equivalent of TT. 7 Sites were collected at the base of the section, one in the monocline and one at the top of the section. From the rest of the lavas we collected one sample each which form one site. In total, we sampled 73 separate flows.
Khatavch (KH)	7	115.4±0.36 Ma	(Barry, 1999)	continuous horizontal section of lavas on top of poorly exposed sediments	Top of the TT-section.
Tsost Magmatic Field (TS)	10	102.9-103.7±0.3 Ma	Barry '99	Basaltic plugs rising up to 200 m above the surrounding region. They are intruded in poorly exposed subhorizontal lavas, mudstones, sandstones and conglomerates.	The basalts are determined to be intrusive on the basis of large scale columnar jointing, the absence of aerial volcanic features and a baked margin around the plugs (Barry, 1999).
Khatan Suudal (KS)	7	57±2.3 Ma	(Devyatkin and Smelov, 1980)	A basaltic plug rising ~100 m above the surrounding peneplain, containing well-developed columnar joints.	The body is determined to be intrusive on the basis of the columnar joints and the absence of flow patterns. No contact with the country rock was exposed and its bedding is unconstrained, but most likely subhorizontal. Its stratigraphic position is unknown.

Table 1: Characteristics and short description of all localities. JU=Jurassic, EC=Early Cretaceous, PC=Post Cretaceous. Italic: ages are estimates, Ar/Ar dating in progress. GPS coordinates of the localities are listed in Table 2

et al., 1993; Vassallo et al., 2005). The restraining bends seem to follow the E-W trending basement grain (Traynor and Sladen, 1995; Cunningham et al., 1996).

In the eastern Gobi-Altai, the stratigraphy is formed by Paleozoic basement which is unconformably covered by extensive Mesozoic and some Cenozoic mafic lavas and continental sediments (Devyatkin and Smelov, 1980; Barry, 1999; Johnson et al., 2001). The Mesozoic deposits comprise some Jurassic lavas (unpubl. map), but the bulk of the stratigraphy is characterised by lower Cretaceous lavas and fluvio-lacustrine deposits. At the Tsost magmatic field, south of Artz Bogd, this stratigraphy is cross-cut by basaltic intrusions of early Cretaceous age (Barry, 1999; Hankard et al., 2006). These sequences are unconformably overlain by upper Cretaceous and Tertiary sediments. Cenozoic formations comprise a rhyolitic plug of unknown age, a basaltic intrusive plug of ±57 Ma (Devyatkin and Smelov, 1980), two lava plateaux of which one is dated at ±30 Ma (Barry, 1999) and a set of Neogene lavas (age dating in progress) filling in Cenozoic topography (Figure 3).

The field area emcompasses three restraining bend uplifts and a stratigraphic column for bounding sequences is given in Figure 4. The stratigraphic position of each locality is indicated and field descriptions for site geology are listed in Table 1. The most complete stratigraphy is found in the Ih Bogd region where Jurassic lavas occur at Dulaan Bogd (DR-Jurassic). Directly to the south, a continuous section of lower Cretaceous lavas and sediments can be traced laterally from Dulaan Bogd to Jaran Bogd (Figure 3) with the base of the Jaran Bogd section (JI) being laterally equivalent to Dulaan Bogd (DR-Cretaceous). This sequence is tilted to the south (12° at Dulaan Bogd, up to 60° at Jaran Bogd) and is unconformably onverlain by alluvial and fluvial sediments of late and post-Cretaceous age which are found at the top of the sections (but were not sampled). West of the Jaran Bogd section, the Paleogene Jaran Plateau (JP) was sampled. Around Jaran Bogd, several lavas infill a Cenozoic topography (Jaran Bogd Neogene (JN) locality), originating from the Jaran Bogd Volcano. The uplift leading to this topography is started in the late Miocene (Howard et al., 2003; Vassallo et al., 2006). The region east of Baga Bogd comprises a stratigraphy of Cretaceous lavas and sediments which is sampled at five localities (Figure 4). The Cenozoic formations sampled in this region comprise the Tsagaanbotga (TB) rhyolitic plug on the southern flanks of Baga Bogd and the 30 Ma Bogd Plateau (BP) (Barry, 1999) east of Baga Bogd. South of Artz Bogd, lower Cretaceous lavas were sampled at the base of the continuous 119-117 Ma Tsagaan Tsav (TT) section (Barry, 1999), its lateral equivalent to the east Kharaat Uul (KU) and some flows in the top of the stratigraphy Khatavch (KH) (115 Ma, Barry, 1999). West of these sections, we sampled a field of basaltic intrusions of 103 Ma in the Tsost Magmatic Field (TS) (Barry, 1999). Finally, south of Baga Bogd, we sampled a 57 Ma (Devyatkin and Smelov, 1980) basaltic intrusion called Khatan Suudal (KS).

In total, we sampled 17 localities (Figure 3). Each locality consists of a minimum of 7 lavas except the Tsagaanbotga locality where we only collected 4 sites, and the Jaran Bogd Neogene locality where we took 7 sites in 3 separate lavas. In the case of successive lavas, we took one site per individual lava. Individual lavas were distinguished based on colour variation, crystal size and weathering profile. For each site, we drilled 7 cores except for the KU-section were we took one sample out of each of ±65 successive lavas. Exact ages of the localities are not always known but good approximations can be made, based on field observations and on an unpublished Russian geological map (anonymous author).

Paleomagnetic Methods

Sampling took place using a water-cooled, gasoline powered motor drill. The orientation of all samples was measured with both a magnetic and a sun compass. To exclude any local mag-

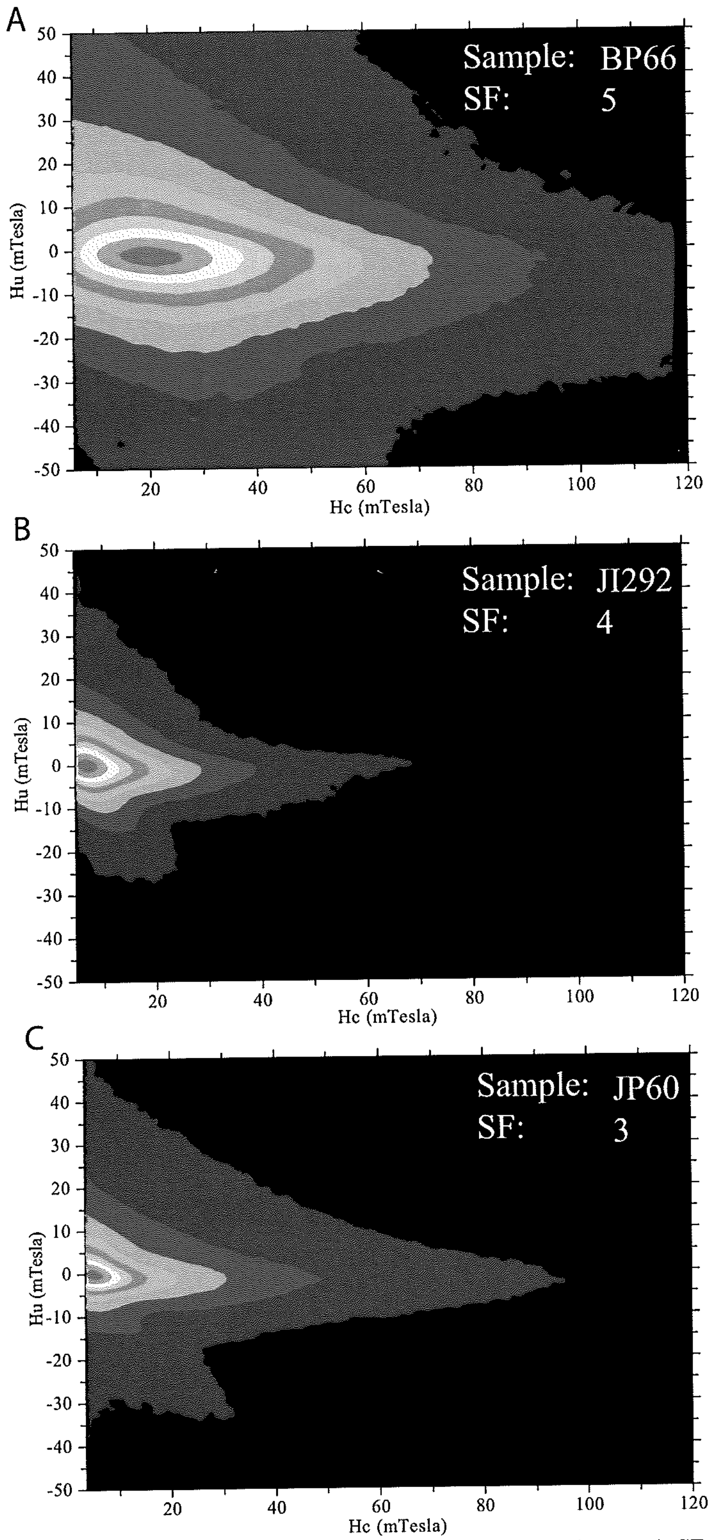

Figure 5: First order reversal curve (FORC) diagrams for three samples (details in text). SF = Smoothing factor which is determined based on the signal/noise ratio. The converging contours indicate the presence of pseudo-single-domain grains.

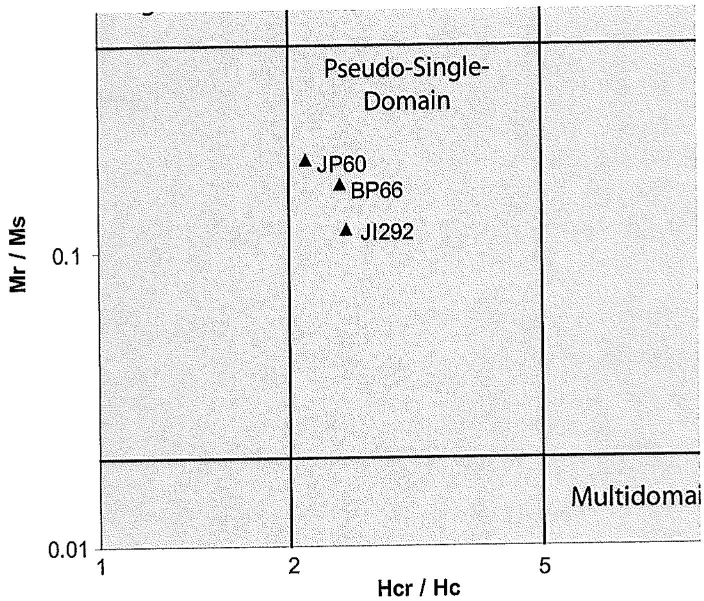

Figure 6: Day-plot of the hysteresis parameters of the studied samples (after Dunlop, 2002).

netic deviations, all paleomagnetic interpretations are based on the solar azimuths. The samples were demagnetised using either thermal (TH) or alternating field (AF) progressive demagnetisation. Heating took place in a magnetically shielded, laboratory-built furnace using small temperature increments of 20 – 80 °C up to temperatures of 640 °C. The AF demagnetisation was carried out with 5 – 20 mT increments up to 120 mT. For all samples, the natural remanent magnetisation (NRM) of the specimens was measured on a 2G Enterprises horizontal DC SQUID cryogenic magnetometer (noise level 3×10-12Am2). For AF demagnetisation, the instrument was interfaced with in-home developed robot-assisted protocols.

To identify the magnetic carriers and their characteristics, acquisition of isothermal remanent magnetization (IRM) was carried out. Samples were carefully selected based on the demagnetisation diagrams. They served as being representative for lightning struck samples (JP60), samples that were entirely demagnetised at ±580 °C (BP66) and at ±560 °C (JI292). Additionally, hysteresis loops were determined, as well as first order reversal curves (FORC). FORC diagrams can identify the contributions of superparamagnetic (SP), single-domain (SD) and multidomain (MD) grains Roberts et al. (2000). The converging contours near the origin (Figure 5)

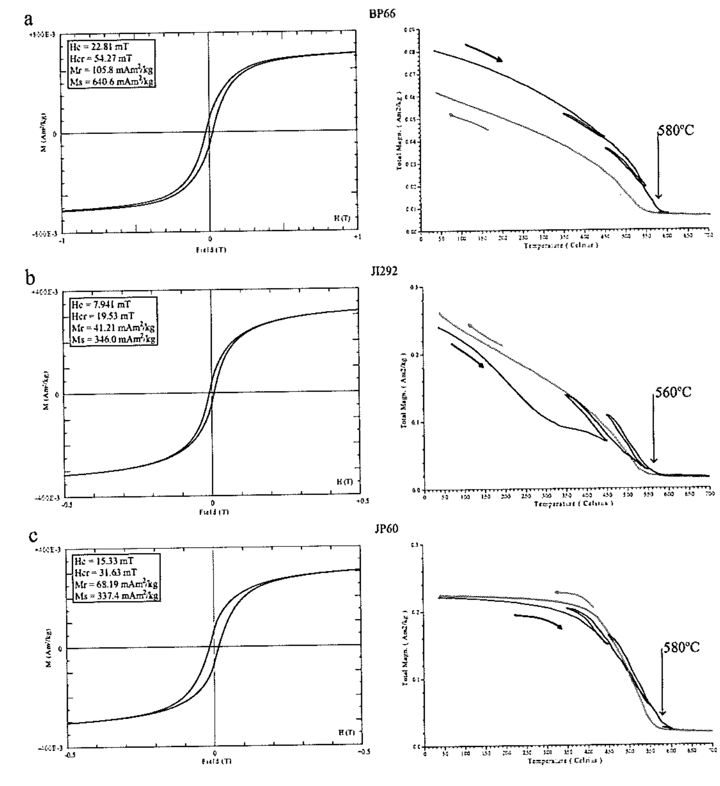

Figure 7: Rock magnetic properties are presented by hysteresis loops and thermomagnetic curves of three different samples. The thin shape of the hysteresis loops indicates the pressence of (pseudo-)single-domain grains. The loops closing at or below 0.3 Tesla in b ans c indicates (titano-)magnetite to be the main carrier. The thermomagnetic curves of the three samples reveal blocking temperatures of 560-580°C which is indicative for (titano-)magnetite to be the main magnetic carrier.

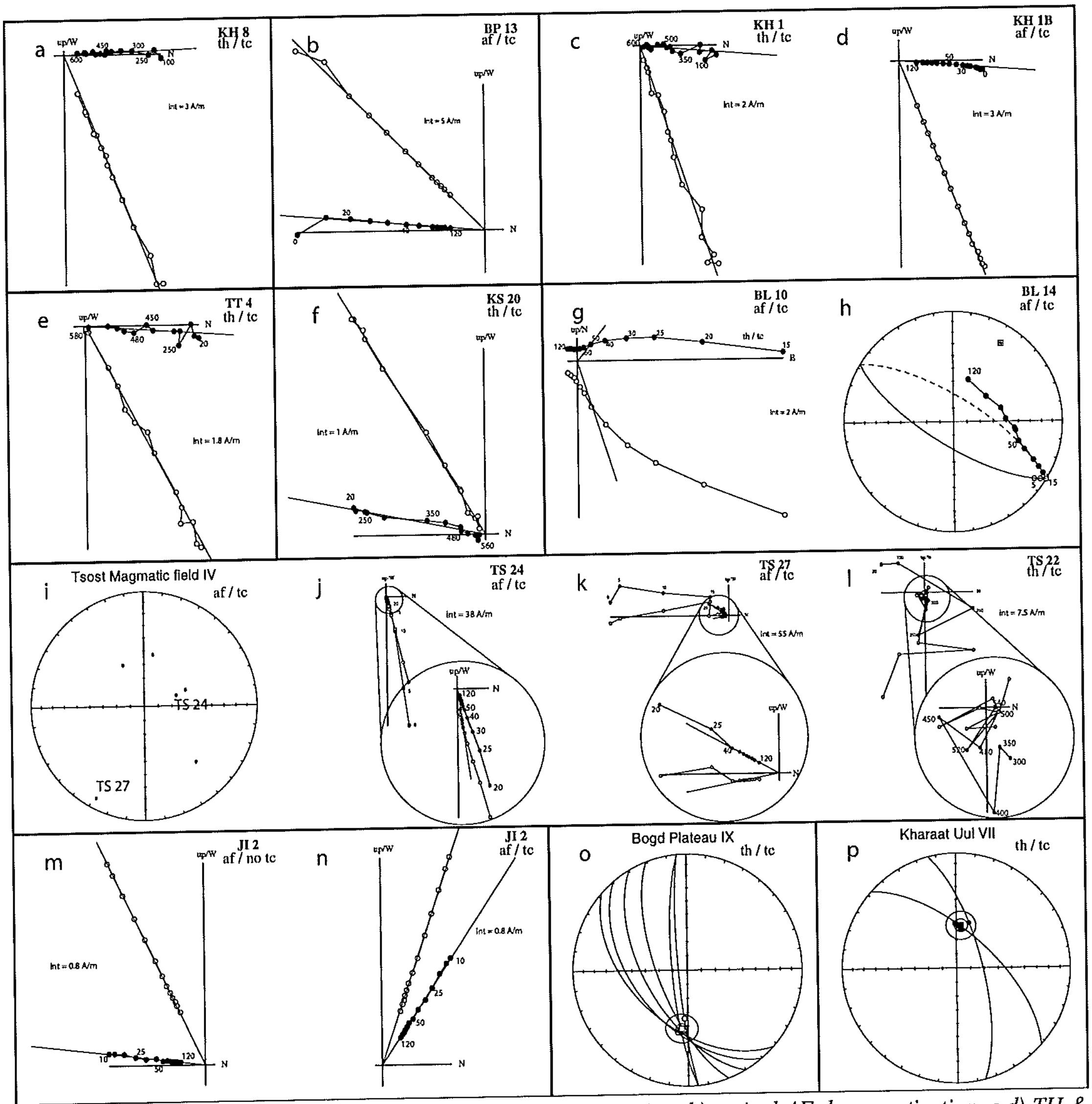

Figure 8: All aspects of demagnetisation. a) typical TH demagnetisation. b) typical AF demagnetisation. c,d) TH & AF result in a comparable direction.. e,f) typical normal (e) and reversed (f) polarity. g) gyro remnent magnetisation. h) dealing with gyro remnent magnetisation by the use of great circles. i)randomness of a lightning struck site with j,k,l being samples from this site, j,k show a good but random magnetisation where l shows a TH totalrandomness. m,n) total remagnetisation of a sample, the reversed direction (m) becomes impossible after tectonic correction (n). o,p)examples of lightning struck rocks where the use of great circles results in a consistent direction.

indicate the presence of pseudo-single-domain (PSD) grains in all three samples. This is confirmed by plotting Mr/Ms against Hhc/Hc in a Day-plot (Day et al., 1977); (Figure 6). Curie temperatures were determined using a modified horizontal translation type Curie balance that applies a cycling field (Mullender et al., 1993). Stepwise increasing temperatures of 450°, 550°, 600°, 650° and 700°C were used revealing blocking temperatures of 560–580 °C (Figure 7). These Curie temperatures, together with the hysteresis loops closing at or below ~0.3 Tesla, indicate (Ti-poor) magnetite to be the main carrier of the natural remanent magnetisation (NRM). Finally, these rock magnetic experiments give us confidence that we measure a stable NRM.

The demagnetisation diagrams of the NRM

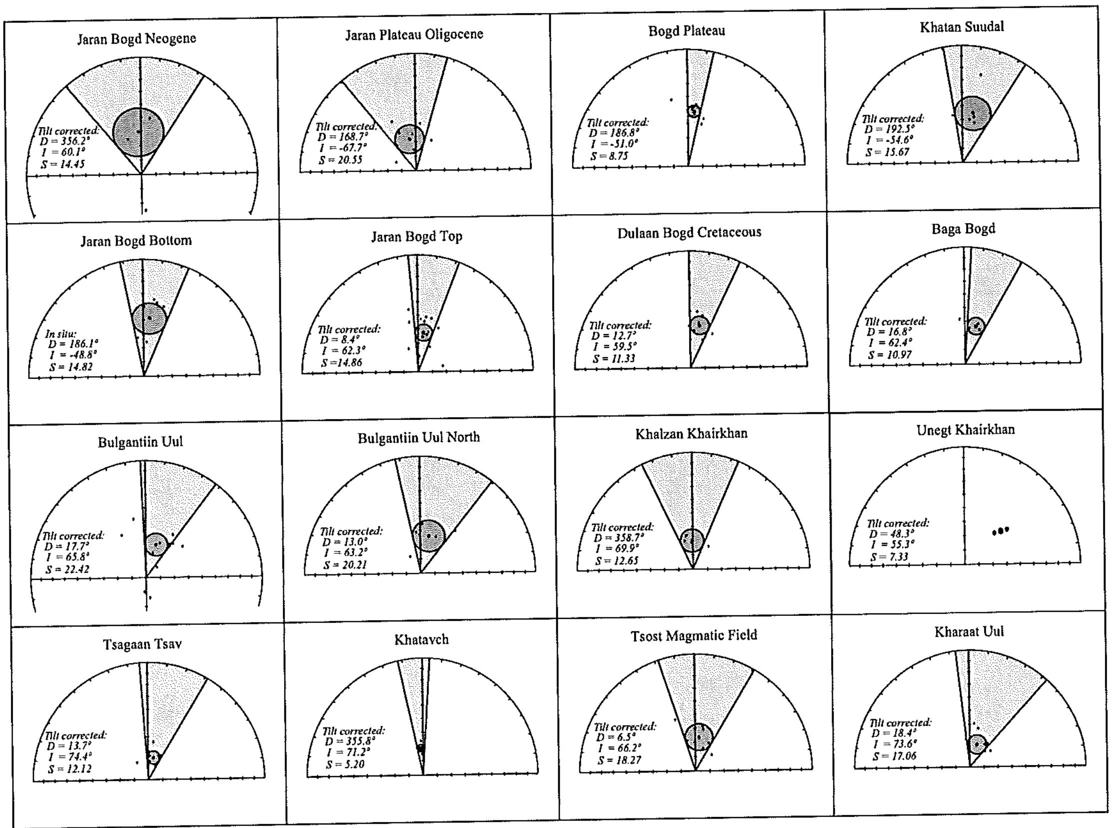

Figure 9: Equal area projections of site and locality mean directions. Closed (open) circles represent normal (reversed) polarities. Onl localities that are used for the analysis have been plotted.

were plotted in orthogonal vector diagrams (Zijderveld, 1967). In addition, a number of multi-component samples were plotted on equal-area projections. Representative examples are given in Figure 8. Identification of the characteristic remanent magnetisation (ChRM) was done by principal component analysis (Kirschvink, 1980). When vector end points showed a trend towards the origin of the diagram, we determined this component to be the ChRM. The resulting directions and statistics from the analysis can be found in Table 2 and Figure 9.

Initially, we demagnetised one sample of every site by thermal demagnetisation. The remaining samples of the sites were either demagnetised on a robotised alternating field demagnetiser or demagnetised thermally, resulting in 492 AF demagnetisation diagrams and 728 TH demagnetisation diagrams. Initial intensities range typically from 0.5-2.0 A/m. The AF demagnetised samples show good agreement with the TH samples of the same site (Figure 8c and 8d). In a number of sites, the ChRM was not recognised in the TH demagnetisation but could clearly be determined in the AF demagnetisation (Figure 8k and 8l).

Samples were rejected from calculating the mean direction if the maximum angular deviation (mad) exceeded 15°. Lava sites were rejected in case of a complete remagnetisation (e.g. caused by lightning) or by exceeding the maximum cut-off angle determined by Vandamme (Vandamme, 1994). These rejected sites are indicated in Table2.

Complete remagnetisation of sites was recognised in 15 cases. The declinations of the lowermost sites of section JI show remarkable deviations from the north after tectonic correction. These sites show consistent reversed directions

Locality Sites	lat	lon	Type	Na	Nc	q	Tilt strike/dip	In Situ D, deg	 I, deg	Tilt Corrected D, deg	 I, deg	k	α95	pol	rot	sense
Cenozoic Sites																
Jaran Bogd Neogene				*3*	*3*	*2*				*356,2*	*60,1*	*51,3*	*17,4*	*n/r*	*4*	*ccw*
JN lava 1 (JN I)	44,8697	100,7193		**7**	**7**	**1**	000/00	-	-	**173,9**	**-64,8**	**196,8**	**4,3**	**r**		
JN lava 2				**4**	**4**	**1**				**9,2**	**49,9**	**104,7**	**9,0**	**n**		
JN II	44,8342	100,8868		7	7	1	000/00	-	-	7,7	47,7	103,1	6,0	n		
JN III	44,8343	100,8860		7	7	1	000/00	-	-	22,7	51,1	87,7	6,5	n		
JN IV	44,8350	100,8864		7	7	1	000/00	-	-	4,2	43,6	304,3	3,5	n		
JN V	44,8344	100,8875		7	7	1	000/00	-	-	2,4	56,2	451,3	2,8	n		
JN lava 3				**5**	**5**	**1**		-	-	**339,4**	**63,7**	**858,7**	**2,6**	**n**		
JN VI	44,8258	100,7902		7	7	1	000/00			334,1	64,3	311,7	3,4	n		
JN VII	44,8261	100,7901		7	7	1	000/00	-	-	337,8	61,4	1103,3	1,8	n		
JN VIII	44,8263	100,7899		7	7	1	000/00	-	-	339,3	63,6	494,7	2,7	n		
JN IX	44,8266	100,7896		7	7	1	000/00	-	-	345,1	66,7	666,8	2,3	n		
JN X	44,8342	100,7896		7	6	1	000/00	-	-	341,4	62,0	963,9	2,1	n		
Jaran Plateau Oligocene				*10*	*8*	*1*		*165,0*	*-65,4*	*168,7*	*-67,7*	*36,4*	*10,1*	*r*	*9*	*cw*
JP I	44,8414	100,6847		7	7	1	065/02	156,2	-59,1	156,3	-61,1	216,6	4,1	r		
JP II	44,8419	100,6847		7	7	1	065/02	173,7	-62,6	175,0	-64,5	877,6	2,0	r		
JP III	44,8433	100,6843	gc	7	7	1	065/02	117,3	-73,5	112,7	-75,0	-	4,9	r		
JP IV	44,8506	100,6764	gc	6	6	2	065/02	143,9	-66,1	143,0	-68,1	-	11,0	r		
JP V	44,8430	100,6735		7	4	1	065/02	172,2	-73,6	174,5	-75,5	88,5	9,8	r		
JP VI	44,8425	100,6707		7	6	2	065/02	203,9	-65,0	207,3	-66,3	41,3	10,5	r		
JP VII	44,8412	100,6715		7	6	1	065/02	183,9	-55,3	185,4	-57,0	144,3	5,6	r		
JP VIII	44,8396	100,6730	gc	7	7	2	065/02	153,9	-49,7	153,8	-51,7	-	14,7	r		
JP IX	44,8391	100,6746		7	7	3	065/02	235,7	-20,2	236,4	-20,5	2,5	48,0	L		
JP X	44,8375	100,6845	gc	7	7	vd	065/02	151,7	75,2	152,1	73,2	-	13,1	n		
Bogd Plateau				*14*	*11*	*1*		183,4	-50,0	*186,8*	*-51,0*	*114,5*	*4,3*	*r*	*7*	*cw*
BP I-VII				**7**	**6**	**1**		**184,2**	**-49,5**	**187,6**	**-50,3**	**387,5**	**3,4**	**r**	**8**	**cw**
BP I	44,7517	102,3084		7	0	3	022/03	-	-	-	-	-	-	L		
BP II	44,7526	102,3068		7	7	1	022/03	185,4	-45,9	188,4	-46,7	176,0	4,6	r		
BP III	44,7529	102,3044		7	6	1	022/03	180,4	-54,0	184,4	-55,0	437,1	3,2	r		
BP IV	44,7524	102,3024		7	7	1	022/03	181,0	-48,3	184,2	-49,3	871,5	2,0	r		
BP V	44,7524	102,2930		7	7	1	022/03	189,4	-52,3	193,3	-52,9	125,1	5,4	r		
BP VI	44,7520	102,2905		7	5	1	022/03	183,6	-50,8	187,2	-51,7	1001,6	2,4	r		
BP VII	44,7517	102,2883		7	7	1	022/03	185,0	-45,2	188,0	-46,0	136,0	5,2	r		
BP VIII-XIV				**7**	**5**	**1**		**182,4**	**-50,7**	**185,9**	**-51,8**	**54,8**	**10,4**	**r**	**6**	**cw**
BP VIII	44,6860	102,2733		7	0	3	027/03	-	-	-	-	-	-	L		
BP IX	44,6861	102,2709	gc	7	7	1	027/03	183,1	-46,7	186,1	-47,8	-	3,8	r		
BP X	44,6863	102,2689		7	6	1	027/03	193,3	-58,4	198,1	-59,0	335,1	3,7	r		
BP XI	44,6853	102,2670	gc	7	7	1	027/03	184,0	-52,0	187,7	-53,1	-	4,3	r		
BP XII	44,6848	102,2584		7	7	1	027/03	194,3	-54,4	198,5	-55,0	109,9	5,8	r		
BP XIII	44,6854	102,2559	gc	7	5	vd	027/03	154,4	-39,0	156,0	-41,4	-	14,9	r		
BP XIV	44,6845	102,2550	gc	7	6	1	027/03	164,2	-39,1	166,1	-41,1	-	3,4	r		
Khatan Suudal				*7*	*6*	*1*				*192,5*	*-54,6*	*34,6*	*12,3*	*r*	*13*	*cw*
KS I	44,4899	101,3380	gc	7	6	3	000/00	-	-	200,6	-55,9	-	15,8	r		
KS II	44,4931	101,3376		7	7	1	000/00	-	-	167,9	-56,3	474,4	2,8	r		
KS III	44,5001	101,3375		7	6	1	000/00	-	-	197,3	-61,1	119,2	6,2	r		
KS IV	44,5008	101,3371		7	7	1	000/00	-	-	194,8	-56,9	184,1	4,5	r		
KS V	44,5011	101,3364	gc	7	6	2	000/00	-	-	192,6	-24,7	-	9,3	r		
KS VI	44,5025	101,3375		7	7	1	000/00	-	-	210,2	-49,7	2261,9	1,3	r		
KS VII	44,5034	101,3377		7	6	1	000/00	-	-	189,5	-59,5	572,7	2,8	r		
Tsagaanbotga				*4*	*2*	*3*				*134,6*	*-46,3*	-	-	*r*	-	-
TB I	44,7424	101,72424	gc	7	6	1	000/00	-	-	154,6	-49,9	-	6,4	r		
TB II	44,7423	101,72404		7	6	3	000/00	-	-	163,3	-43,2	12,1	20,0	r		
TB III	44,7424	101,72386		7	6	3	000/00	-	-	225,2	-54,1	6,8	27,8	r		
TB IV	44,7421	101,72395		7	6	1	000/00	-	-	117,9	-39,7	55,5	9,1	r		
Cretaceous Sites																
Jaran Bogd Cretaceous				*27*	*16*	*1*		*8,0*	*12,6*	*8,4*	*62,3*	*40,0*	*6,0*	*n*	*8*	*cw*
JI I	44,8383	100,7260		7	6	3	062/50	185,2	-66	307,1	-58,0	442,6	3,2	o		
JI II	44,8679	100,7255		7	7	3	062/50	180,2	-61,5	302,7	-62,5	394,6	3,0	o		
JI III	44,8678	100,7258		7	6	3	040/22	171,1	-62,8	222,6	-72,5	446,7	3,2	o		
JI IV	44,8763	100,7253		7	7	3	040/22	188,2	-34,5	204,8	-43,5	35,5	10,3	o		
JI V	44,8596	100,7258		7	6	3	040/22	196,8	-38,2	215,6	-43,6	52,3	9,3	o		

Table 2: Site & Locality mean directions after NRM analysis of all samples. Type=type of identification of ChRM, only great circle method is indicated (gc), Na=number of analised samples, Nc=number of conclusive samples, q=quality factor based on the k-value (1=conclusive, 2= indicative, 3=rejected, for criteria see text), k=Fisher's precision parameter (Fisher, 1953), α95=95% cone of confidence, pol=polarity (n=normal, r=reversed, o=complete remagnetised, L=lightning induced magnetisation), rot=amount of rotation, sense=sense of rotation (cw=clockwise, ccw=counterclockwise).

Table 2: continued

Locality Sites	lat	lon	Type	Na	Nc	q	Tilt strike/dip	In Situ D, deg	In Situ I, deg	Tilt Corrected D, deg	Tilt Corrected I, deg	k	α95	pol	rot	sense
JI VI	44,8596	100,7261		7	6	3	040/22	180,8	-40,3	200,9	-51,3	346,2	3,6	o		
JI VII	44,8595	100,7263		7	5	3	032/34	190,8	-36,5	219,0	-41,0	80,9	8,6	o		
JI VIII	44,8595	100,7265		7	0	3	032/34	-	-	-	-	-	-	o		
JI IX	44,8595	100,7334		7	0	3	032/34	-	-	-	-	-	-	o		
JI X	44,8591	100,7266		7	0	3	032/34	-	-	-	-	-	-	o		
JI XI	44,8581	100,7406		7	4	1	045/15	349,9	54,4	8,0	65,4	58,9	12,1	n		
JI XII	44,8504	100,7418		7	0	3	040/16	-	-	-	-	-	-	o		
JI XIII	44,8407	100,7394		7	5	1	110/88	355,4	-36,4	351,6	45,3	74,7	8,9	n/r		
JI XIV	44,8387	100,7414	gc	7	7	1	050/16	342,5	40,1	350,2	54,5	-	4,3	n		
JI XV	44,8369	100,7422		7	7	1	082/19	15,6	39,1	25,6	55,9	271,4	3,7	n		
JI XVI	44,8339	100,7584	gc	7	6	1	100/40	11,9	23,2	13,8	63,2	-	3,7	n		
JI XVII	44,8256	100,7686		7	7	1	069/30	351,7	30,7	0,8	59,5	510,4	2,7	n		
JI XVIII	44,8204	100,7915		7	6	1	112/64	16,2	1,9	7,9	65,3	884,0	2,3	n		
JI XIX	44,8202	100,7916		7	7	1	113/60	13,8	-4,7	7,2	54,2	241,9	3,9	n		
JI XX	44,8201	100,7916		7	7	2	113/60	17,8	-8,6	14,8	51,1	32,4	10,8	n		
JI XXI	44,8200	100,7916		7	6	1	113/60	10,1	17,2	337,3	72,6	82,8	7,4	n		
JI XXII	44,8199	100,7917		7	7	1	113/60	14,1	-8,2	9,0	50,9	297,0	3,5	n		
JI XXIII	44,8199	100,7915		7	4	1	113/60	11,2	-5,5	3,4	52,7	126,9	8,2	n		
JI XXIV	44,8197	100,7915		7	7	1	112/60	18,6	1,6	14,9	61,4	167,4	4,7	n		
JI XXV	44,8194	100,7917		7	6	1	112/70	16,5	1,3	25,7	70,8	302,4	3,9	n		
JI XXVI	44,8192	100,7911		7	7	1	112/70	28,5	11,8	77,1	72,2	1073,2	1,8	n		
JI XXVII	44,8168	100,7858		7	7	1	083/40	355,2	38,9	4,8	78,7	491,8	2,7	n		
Dulaan Bogd Cretaceous				***7***	***7***	***1***		***11,0***	***47,6***	***12,7***	***59,5***	***87,6***	***6,5***	***n***	***13***	***cw***
DR XI	44,9090	101,0416		7	5	1	096/12	25,9	50,6	33,1	61,6	127,4	6,8	n		
DR XII	44,9088	101,0407		7	7	1	096/12	10,0	45,7	11,2	57,7	99,0	6,1	n		
DR XIII	44,9087	101,0401		7	4	1	096/12	0,3	48,5	358,3	60,4	80,9	10,3	n		
DR XIV	44,9085	101,0386		7	5	1	096/12	6,3	51,6	6,4	63,6	201,0	5,4	n		
DR XV	44,9059	101,0384		7	7	1	096/12	17,9	57,0	23,9	68,6	79,9	6,8	n		
DR XVI	44,9057	101,0395		7	5	1	096/12	12,1	40,2	13,6	52,1	68,9	9,3	n		
DR XVII	44,9061	101,0419		7	7	1	096/12	7,1	37,8	7,4	49,8	504,0	2,7	n		
Baga Bogd				***7***	***6***	***1***		***12,8***	***52,7***	***16,8***	***62,4***	***122,0***	***6,1***	***n***	***17***	***cw***
BA I	44,7705	101,8514		7	5	1	090/10	18,0	54,4	24,0	63,8	408,2	3,8	n		
BA II	44,7693	101,8512		7	7	1	090/10	22,7	50,7	29,0	59,7	108,0	5,8	n		
BA III	44,7686	101,8508		7	6	1	090/10	354,9	48,3	353,5	58,2	103,2	6,6	n		
BA IV	44,7673	101,8502		7	6	1	090/10	5,3	54,8	7,2	64,7	140,1	5,7	n		
BA V	44,7672	101,8416		7	7	1	090/10	14,6	50,8	18,8	60,4	138,1	5,2	n		
BA VI	44,7672	101,8376		7	6	1	090/10	22,7	54,6	30,1	63,6	189,7	15,2	n		
BA VII	44,7673	101,8361		7	6	3	090/10	6,8	33,1	7,8	43,0	21,6	14,8	n		
Bulgantiin Uul				***15***	***13***	***2***		***4,9***	***58,6***	***17,7***	***65,8***	***27,5***	***8,0***	***n/r***	***18***	***cw***
base				**10**	**9**	**1**		**358,5**	**57,2**	**4,2**	**68,5**	**30,8**	**9,4**	**n/r**		
BL I	44,7921	101,9531		7	6	1	073/12	347,3	35,4	348,2	47,4	134,1	5,8	n		
BL II	44,7912	101,9525	gc	7	6	1	073/12	333,2	43,6	330,5	55,4	-	3,8	n		
BL III	44,7905	101,9522		7	6	1	073/12	23,0	52,5	36,3	60,8	330,8	3,7	n		
BL IV	44,7896	101,9507		7	0	3	077/10	-	-	-	-	-	-	o		
BL V	44,7758	101,9523		7	6	1	077/10	6,0	62,8	15,8	72,0	233,5	4,4	n		
BL VI	44,7741	101,9530	gc	7	7	1	077/10	357,1	46,4	359,6	56,2	-	7,7	n		
BL VII	44,7730	101,9527		7	6	1	077/10	13,9	55,2	22,7	63,8	774,9	2,4	n		
BL VIII	44,7720	101,9536		7	7	1	077/10	18,2	72,1	46,6	79,4	572,6	2,5	n		
BL IX	44,7695	101,9538	gc	7	6	1	090/15	176,8	-70,5	186,5	-80,2	-	5,6	r		
BL X	44,7683	101,9539	gc	7	6	1	077/09	168,1	-66,9	168,8	-75,9	-	4,2	r		
section				**5**	**4**	**1**		**22,5**	**60,5**	**41,4**	**58,8**	**233,7**	**6,8**	**n**		
BL XI	44,7676	101,9383		7	0	3	094/11	-	-	-	-	-	-	o		
BL XII	44,7552	102,0059		7	6	1	031/12	31,7	58,1	50,1	56,0	268,3	4,1	n		
BL XIII	44,7538	102,0086		7	5	2	025/13	14,6	53,9	32,7	54,2	39,0	12,4	n		
BL XIV	44,7529	102,0247		7	7	1	030/10	18,7	62,3	38,0	62,6	247,8	3,8	n		
BL XV	44,7539	102,0347		7	7	1	007/11	20,8	64,0	39,8	59,6	356,1	3,2	n		
Bulgantiin Uul North				***7***	***7***	***1***		**211,6**	**43,8**	***13,0***	***63,2***	***32,8***	***11,2***	***n***	***13***	***cw***
BN I	44,8096	102,0090		7	6	1	116/70	196,9	47,7	38,8	61,3	93,1	7,0	n		
BN II	44,8170	102,0072	gc	7	5	1	116/70	189,3	56,9	40,5	51,1	-	6,9	n		
BN III	44,8172	102,0067	gc	7	7	1	116/70	222,9	43,5	358,8	62,6	-	6,5	n		
BN IV	44,8173	102,0059	gc	7	7	1	116/70	226,7	43,2	353,9	61,0	-	3,9	n		
BN V	44,8177	102,0046	gc	7	6	1	116/70	219,0	27,0	328,7	76,2	-	4,0	n		
BN VI	44,8179	102,0038	gc	7	6	2	110/80	197,9	37,8	23,6	62,1	-	8,6	n		
BN VII	44,8187	102,0019	gc	7	6	1	110/80	213,6	42,8	2,5	55,1	-	6,3	n		
Khalzan Khairkhan				***7***	***5***	***1***		**350,8**	**66,0**	***358,7***	***69,9***	***107,3***	***8,1***	***n***	***1***	***ccw***
KK I	44,7208	102,0697		7	7	3	045/05	292,7	77,5	279,4	81,9	15,7	15,7	n		

Table 2: continued

Locality Sites	lat	lon	Type	Na	Nc	q	Tilt strike/dip	In Situ D, deg	In Situ I, deg	Tilt Corrected D, deg	Tilt Corrected I, deg	k	α95	pol	rot	sense
KK II	44,7204	102,0688	gc	7	5	1	045/05	339,1	64,7	344,4	69,2	-	7,0	n		
KK III	44,7199	102,0687		7	6	2	045/05	345,0	61,5	350,5	65,7	30,8	12,3	n		
KK IV	44,7185	102,0680		7	7	1	045/05	21,4	69,1	34,5	70,6	253,9	3,8	n		
KK V	44,7181	102,0682		7	0	3	045/05	-	-	-	-	-	-	L		
KK VI	44,7185	102,0688		7	7	1	045/05	349,4	67,5	357,7	71,4	221,0	4,1	n		
KK VII	44,7189	102,0695		7	6	1	045/05	343,2	61,6	348,4	65,9	790,1	2,4	n		
Unegt Khairkhan				***7***	***2***	***1***		***73,8***	***67,0***	***48,3***	***55,3***	-	-	***n***	-	-
UK I	44,6563	102,1002		7	0	3	322/40	-	-	-	-	-	-	L		
UK II	44,6574	102,0926	gc	7	7	3	322/40	254,8	22,6	253,7	-14,6	-	14,3	L		
UK III	44,6588	102,0914		7	6	vd	322/40	238,8	4,6	241,5	44,2	55,1	9,1	n		
UK IV	44,6839	102,0567	gc	7	6	1	322/40	73,5	-88,9	51,4	51,0	-	9,4	n		
UK V	44,6764	102,0583		7	6	vd	322/40	177,9	74,6	75,3	57,0	197,7	4,8	n		
UK VI	44,6753	102,0681	gc	7	6	1	322/40	253,4	79,5	44,5	59,6	-	9,2	n		
UK VII	44,6897	102,0185		7	0	3	120/40	-	-	-	-	-	-	L		
Tsagaan Tsav				***10***	***9***	***1***		***2,9***	***65,1***	***13,7***	***74,4***	***128,2***	***4,6***	***n***	***14***	***cw***
TT I	44,4021	102,4217		7	7	1	075/10	2,3	53,9	8,0	63,3	218,7	4,1	n		
TT II	44,4018	102,4221		7	6	1	075/10	9,5	69,1	28,1	77,5	134,7	5,8	n		
TT III	44,4017	102,4221	gc	7	7	3	075/10	321,9	75,2	287,3	83,2	-	31,2	o		
TT IV	44,4008	102,4224		7	7	1	075/10	333,9	65,9	326,5	75,6	692,3	2,3	n		
TT V	44,4005	102,4223	gc	7	5	1	075/10	356,3	67,5	4,8	77,2	-	3,4	n		
TT VI	44,3927	102,4219		7	5	1	075/10	12,7	65,0	27,9	73,2	123,7	6,0	n		
TT VII	44,3923	102,4212		7	7	1	075/10	15,2	62,6	29,3	70,6	168,4	4,7	n		
TT VIII	44,3913	102,4207	gc	7	7	1	075/10	357,2	63,9	4,2	73,5	-	5,2	n		
TT IX	44,3906	102,4211		7	6	1	075/10	10,4	63,5	23,4	72,0	1290,6	1,9	n		
TT X	44,3889	102,4204		7	7	1	075/10	6,9	70,7	26,6	79,3	630,5	2,4	n		
Khatavch				***7***	***7***	***1***				***355,8***	***71,2***	***599,0***	***2,5***	***n***	***4***	***ccw***
KH I	44,3030	102,4035		7	6	1	000/00	-	-	355,4	72,8	108,8	6,5	n		
KH II	44,3023	102,4035		7	6	1	000/00	-	-	356,6	66,0	554,2	2,8	n		
KH III	44,3019	102,4035		7	7	1	000/00	-	-	347,0	70,6	437,6	2,9	n		
KH IV	44,3008	102,4035		7	7	1	000/00	-	-	352,2	70,7	245,3	3,9	n		
KH V	44,2933	102,4038		7	7	1	000/00	-	-	357,0	75,4	292,4	2,7	n		
KH VI	44,2929	102,4038		7	7	1	000/00	-	-	3,8	70,7	756,7	2,2	n		
KH VII	44,2926	102,4030		7	7	1	000/00	-	-	358,6	71,8	294,4	3,5	n		
Tsost Magmatic Field				***10***	***7***	***1***				***6,5***	***66,2***	***41,7***	***9,5***	***n***	***7***	***cw***
TS I	44,2884	102,3413		7	7	1	000/00	-	-	25,5	68,3	200,3	5,4	n		
TS II	44,2860	102,3225		7	5	1	000/00	-	-	45,1	74,0	579,5	3,2	n		
TS III	44,2568	102,1693	gc	7	6	1	000/00	-	-	19,3	73,4	-	5,4	n (L)		
TS IV	44,2574	102,1842		7	0	3	000/00	-	-	-	-	-	-	L		
TS V	44,2546	102,1861		7	0	3	000/00	-	-	-	-	-	-	L		
TS VI	44,2715	102,2012	gc	7	?	1	000/00	-	-	345,6	68,3	-	6,2	n (L)		
TS VII	44,2718	102,2013		7	6	1	000/00	-	-	9,6	58,2	2354,2	1,4	n		
TS VIII	44,2742	102,1927	gc	7	6	1	000/00	-	-	338,8	51,0	-	4,0	n (L)		
TS IX	44,2762	102,1903		7	6	1	000/00	-	-	11,1	60,1	159,4	5,3	n		
TS X	44,2838	102,1895		7	6	vd	000/00	-	-	33,9	-25,7	285,0	4,0	r		
Kharaat Uul				***9***	***9***	***1***		***22,9***	***71,0***	***18,4***	***73,6***	***60,3***	***6,7***	***n***	***18***	***cw***
KU I	44,4538	102,6255		7	6	1	110/10	10,6	69,7	2,0	79,4	439,4	3,7	n		
KU II	44,4526	102,6254		7	5	1	110/10	8,3	69,5	357,9	79,1	133,7	6,6	n		
KU III	44,4519	102,6252		7	7	1	110/10	27,0	75,7	42,4	85,5	551,5	2,6	n		
KU IV	44,4514	102,6248		7	7	1	135/11	37,7	60,1	33,8	71,0	624,3	2,4	n		
KU V	44,4504	102,6222		7	6	1	110/08	36,8	67,3	45,1	74,8	431,6	3,2	n		
KU VI	44,4379	102,6208		7	7	1	110/08	43,4	64,3	52,6	71,4	81,1	6,7	n		
KU VII	44,4354	102,6230	gc	7	5	1	125/06	10,5	53,9	6,4	59,3	-	4,6	n		
KU VIII	44,4034	102,6097		7	7	1	100/50	201,3	58,1	352,0	70,5	377,9	3,1	n		
KU IX	44,2764	102,7864		7	7	1	085/05	10,6	57,5	13,1	62,3	262,8	3,7	n		
KU section	-	-		65	59	3	-	-	-	37,3	69,1	19,1	4,4	n		
								Jurassic Sites								
Dulaan Bogd Jurassic				***10***	***8***	***3***		***182,1***	***-10,5***	***213,7***	***-75,6***	***5,3***	***26,6***	***n/r***	-	-
DR I	44,9253	101,0585		7	7	1	095/45	197,0	-6,284	203,7	-49,9	205,6	4,2	r		
DR II	44,9253	101,0586		7	6	1	095/75	201,3	-14,1	273,8	-74,2	287,2	3,6	r		
DR III	44,9250	101,0586		7	0	3	095/75	-	-	-	-	-	-	o		
DR IV	44,9244	101,0591		7	7	1	095/75	200,9	-8,348	253,6	-73,1	710,1	2,3	r		
DR V	44,9234	101,0597		7	7	1	095/75	41,2	22,761	113,4	55,0	110,9	5,8	n		
DR VI	44,9232	101,0599		7	7	1	055/55	45,2	61,605	110,2	34,8	385,9	3,1	n		
DR VII	44,9230	101,0670		7	6	1	060/70	134,3	25,2	130,7	-42,3	127,0	6,0	r		
DR VIII	44,9230	101,0673		7	6	1	060/70	149,8	2,2992	149,5	-67,7	51,6	9,4	r		
DR IX	44,9229	101,0678		7	6	1	070/65	145,0	9,6454	135,3	-52,4	298,5	3,9	r		
DR X	44,9226	101,0684		7	6	3	070/65	129,0	21,119	124,1	-34,9	19,5	15,6	r		

before tectonic correction and we interpreted this as a post-folding obtained NRM, which is confirmed by the negative result of the foldtest sensu Tauxe and Watson (1994); (Figure 10a). The overprint is probably related to post-tilting volcanism of the Jaran Bogd volcano (Figure 3). Nine sites show complete remagnetisation caused by lightning. Lightning has a strong influence on the magnetisation of rocks: the NRM of rocks struck by lightning can be entirely or partly overprinted (Hallimond and Herroun, 1933). The identification of lightning-induced NRM has been based on the high intensities found in these samples. No clear correlation could be shown between the intensity decay of lightning struck rocks and rocks unaffected by lightning as has been suggested by Strik (2004). Rejection of sites was thus based on the unusually high intensities together with the within-site randomness of the NRM directions (Figure 8i). In some cases, an overprint caused by lightning or gyroremanent remagnetisation could be identified and eliminated. This was done using the great circle method: great cicles were drawn when clearly recognised, setpoints were determined when possible (representative examples in Figure 8). Common true mean directions (ctmd) were tested using the reversal test of McFadden and McElhinny (1988), based on the statistics of McFadden and Lowes (1981).

A quality measure was used for sites that showed a low coherency to reject them from the calculation of the mean direction of the locality, which is indicated by a quality factor (q) of 1 to 3 (indicated in Table 2). We rejected lava sites with k-values < 30 (q = 3) and weighted the sites at 50% when 30 < k < 50 (q = 2). Four sites showed a k-value below 30 (or α95 > 15°) and were therefore rejected, eight sites are weighted for 50%. To calculate a site mean direction, multiple samples within one lava are required. Accordingly, we excluded all samples of the KU-section from further interpretation. The locality DR-Jurassic is excluded from further analysis because of its scattered directions (k=5.3) and the poor age constraint. Also the TB rhyolitic plug was rejected because of its very weak signal and scattered paleomagnetic directions. Finally, we applied a cutoff angle based on Vandamme (1994) to determine the angular standard deviation (ASD). This was done for the Cenozoic localities individually and for the Cretaceous samples on all remaining sites together. In to-

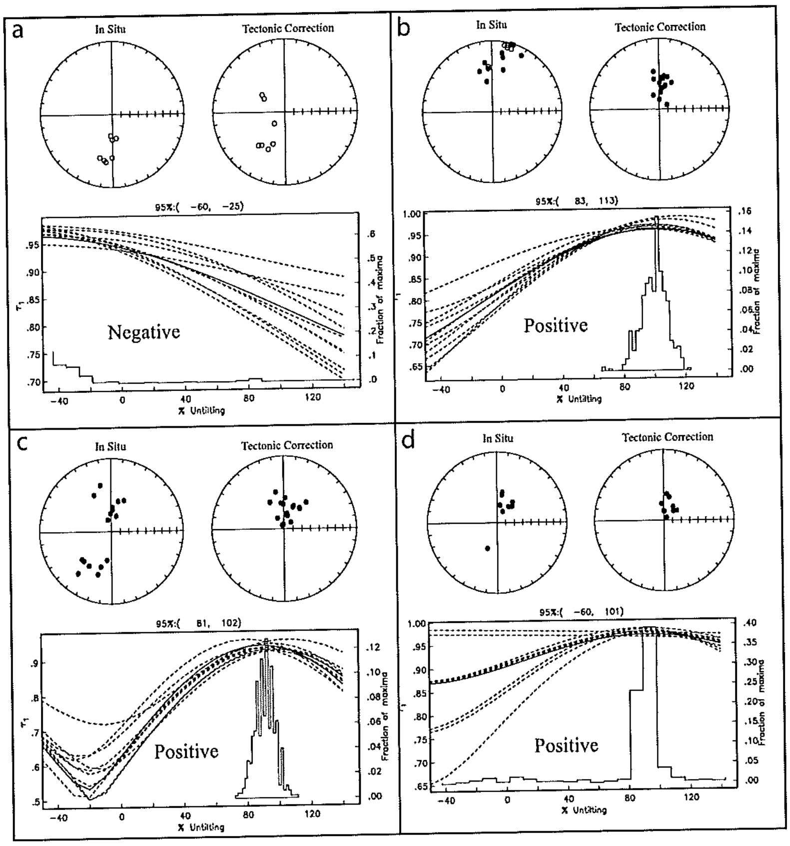

Figure 10: Results from the foldtests of Tauxe and Watson (1994). Equal area projcetions show the site mean directions before and after unfolding of a) the bottom 7 sites of the JI locality (negative) b) the top 15 sites of the JI sections (positive) c) the localitites BL and BN (positive) d) the KU locality (positive).

tal, five sites were rejected when they exceeded this angle (Table 2).

To test whether the ChRM is the original NRM obtained before folding, 4 foldtests were carried out in 3 different regions. The top of the JI section, the localities BL and BN and the sites of the KU locality pass the foldtests of both McFadden (1990) and Tauxe and Watson (1994); (Figure 10b-d). The best results are with 95% confidence between 90–114, 81–102 and -60–101 percent of unfolding for the JI, BL-BN and the KU localities respectively. As can be seen from Figure 10, the foldtest in the KU locality is highly dominated by one site. Still it can be concluded that the NRM of each area tested is obtained prior to folding. Because the sampled Cretaceous lavas were almost all deposited during the Cretaceous Normal Superchon, we could not carry out a reversal test.

To investigate the similarity between Cretaceous localities, 11 tests were applied to determine whether they contain a ctmd. Localities of the same area were tested as well as (sets of) localities of different areas (Table 3). The tests used the McFadden and McElhinny (1990) classification of the reversal test where we made one locality to be reversed each time. With 10 tests, the angle between the means of the (sets of) localities is below the critical angle indicating that they passed the test and show a ctmd. The last test is negative which means that areas a&b do not have a ctmd with area c. This indicates that we should evaluate these areas seperately. However, untill we have better age determinations we assume that the Cretaceous directions are undistinguishable and we calculate a mean ChRM-direction and its corresponding pole for all localities.

In addition to the Cretaceous direction, we calculated Cenozoic mean directions for the localities JN, JP, BP and KS. We adopted the criterion that a minimum of seven sites is required to calculate a pole. Because of the small amount of individual lavas, it is not possible to calculate

		γ	γ_c	Classification
area a (SE of Ih Bogd):				
JI-section	JI-top	7.5	12.1	B
JI	DR	3.2	8.5	A
area b (S+SE of Baga Bogd):				
BA	BL	7.4	11.1	B
BA	BN	1.6	11.6	A
BL	BN	5.9	13.6	B
BA&BL&BN	KK&UK	7.0	8.3	B
area c (S of Artz Bogd):				
TT	TS	8.5	9.9	B
TT&TS	KH	4.6	5.4	A
TT&TS&KH	KU	4.6	7.5	A
all:				
a	b	4.5	6.0	A
a&b	c	8.2	4.3	NEG

Table 3: Cretaceous localities are tested for a common true mean direction, after the statistics of McFadden and Lowes (1981).

a reliable pole for the locality JN. The localities JP and BP, which are supposed to be of the same age beceause of their field appearence, share a common true mean direction. The paleo-poles of this study are plotted together with the reference apparent polar wander paths of Besse and Courtillot (2002), Schettino and Scotese (2005) and Torsvik et al. (2006); (Figure 11).

Analysis

Quality control

The interpretations of our data are hampered by limited age constraints on the sampled lavas because 40Ar/39Ar dating has not yet been finalised. At five localities, the published rock age is within a narrow range of 1 Myr which is accurate enough for a paleomagnetic analysis according to the reliability criteria assigned by Van der Voo (1990). The other ages are to be obtained but field-based estimates will be used until that time. From the applied foldtests, it can be concluded that the ChRM is the original NRM and was acquired before tilting, and most probably acquired during formation of the rock. Preliminary palynologic results from Dulaan Bogd and Jaran Bogd suggest a timespan from Hauterivian to late Albian (van Hinsbergen et al., in prep.). In the volcanic deposits, single lavas represent spot readings of the earth magnetic field. The presence of a reversed direction in the Bulgantiin Uul (BL) section and the intercalated clay-layers in

APWP of Eurasia

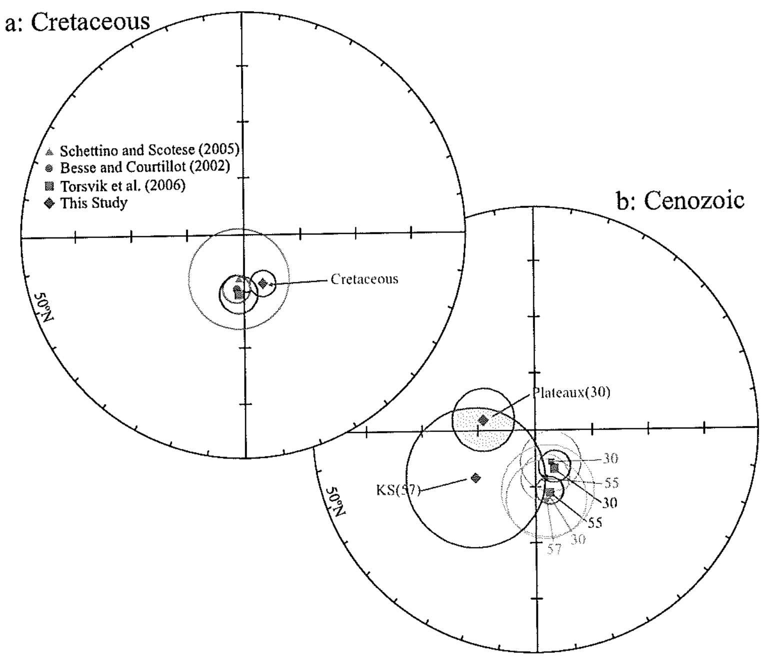

Figure 11: Paleopoles obtained from this study are plotted together with the averaged reference APWPs of Besse and courtillot (2002), Schettino and Scotese (2005) and Torsvik et al. (2006) with their a95 circles of confidence for the Cretaceous (a) and the Cenozoic (b). a: the BC02 path is averaged for 130-95 Ma, the SC05 path is averaged for 120-96 Ma and the TO06 path is averaged for 130-90 Ma. b: two poles of this study with their ages (Ma) are plotted together with the reference poles for equivalent ages.

the Cretaceous dataset indicate that enough time has elapsed for secular variation to be averaged (Van der Voo, 1990). For the Cretaceous series the angular standard deviation of all 88 sites is $S\lambda=18.0°$ ($Sl=16.5°$, $Su=19.8°$) which corresponds to the scatter modelled by McFadden et al. (1991) of $S\lambda=16.9°$ ($Sl=14.9°$, $Su=19.5°$) for 40-50° latitude for the 80-110 Ma period (Figure 12). Our data do not fit the 110-195 Ma curve, but they plot at the intersection of the 0-5 Ma and the 80-110 Ma curves. Hence, our data do not indicate any difference in paleosecular variation during the Cretaceous normal superchron (CNS) with respect to the last 5 Myr.

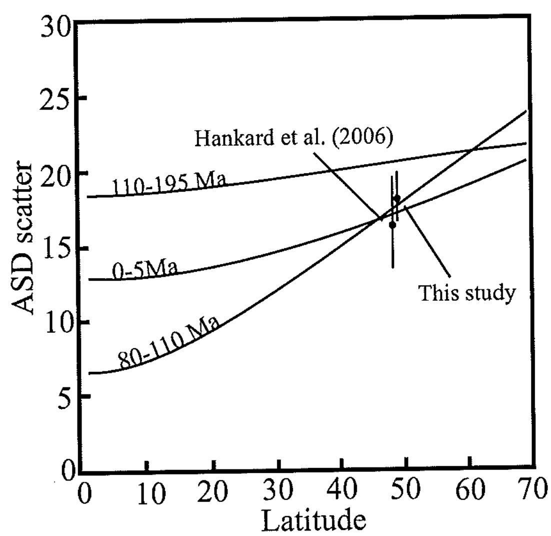

Figure 12: ASD scatter of this study is plotted together with the results of Hankard et al. (2006) and the prediction for paleosecular variation after model G of McFadden et al. (1991) for three different time windows.

Cretaceous Pole

The ctmd for the Cretaceous localities leads to a polar wander path for the Gobi-Altai for the timespan 130-95 Ma. This period falls within the Cretaceous standstill reported by Besse and Courtillot (2002) and our data constrain this by showing that no significant plate motion has occurred during this period. From the 88 remaining Cretaceous sites a mean direction of D=12.3° and I=66.5° (k=43.4 α95=2.3) is obtained which corresponds to a paleo-pole of λ=80.6°N, φ=160.0°E (α95=2.3). This Cretaceous Gobi-Altai pole coincides with the reference APWP's for the continent of Eurasia of Besse and Courtillot, 2002 (BC02), Schettino and Scotese, 2005 (SC05) and Torsvik et al., 2006 (TO06); (Figure 11). Our pole is plotted together with the mean pole of the reference path for a 130-95 age window and shows good correspondence ($\Delta\lambda$=0.3°, $\Delta\lambda$=1.4° and $\Delta\lambda$=1.2° with BC02, SC05 and TO06 respectively.

The early Cretaceous APWP constrains the path of Mongolia (Enkin et al., 1992). Figure 13 shows that our Cretaceous pole corresponds well with the previously published data for Mongolia and with the path of the North China Block. This confirms that Mongolia joined the North and South China terranes during pre-Cretaceous times (Enkin et al., 1992; Pruner, 1992) and consequently followed the same path since.

The fact that our early Cretaceous APWP for Mongolia coincides with the reference path for Eurasia means that the Gobi-Altai region was connected to the Eurasian plate and acted as a rigid plate since the late Cretaceous. This confirms that the Mongol-Ochotsk ocean was closed by the end of the Jurassic and Mongolia followed the Eurasian polar wander since late Jurassic (Zonenshain et al., 1990; Enkin et al., 1992; Van der Voo et al., 1999). Our results reject any suggestion for post Cretaceous large scale relative motion between Mongolia and Siberia postulated by Cogné et al. (2005, 1999) and Hankard et al. (2005).

APWP of Mongolia and the North China Block (NCB)

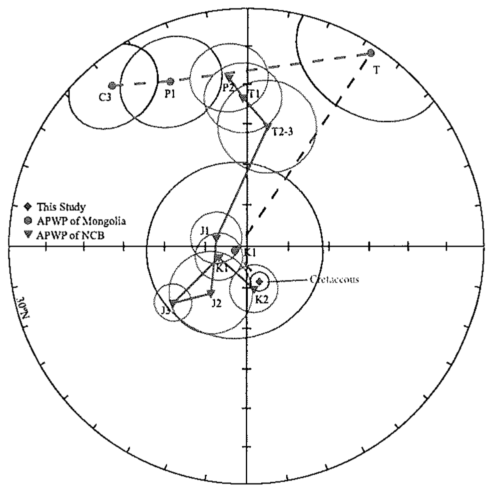

Figure 13: The Cretaceous paleopole obtained from this study is plotted together with the APWPs of Mongolia and the North China Block (NCB) with their α95 elipses of confidence obtained from Enkin et al. (1992). Ages are indicated: C=Carboniferous, P=Permian, T=Triassic, J=Jurassic, K=Cretaceous.

Cenozoic Poles

The directions of the two plateaux, near Jaran Bogd (JP) and Baga Bogd (BP), combine into one reversed common true mean direction of D=180° and I=-55.9° (k=38.6 α95=5.5); (Figure 11) which shows there has been no rotation since deposition. The inclination is 10°±7.6 lower when compared to the expected inclination obtained from the reference APWP of Besse and Courtillot (2002). Accordingly, the resulting paleopole of the plateaux shows no correspondence with the reference pole of 30 Ma. This may indicate that the localities contain too few lavas to average out paleosecular variation. The 95% confidence cone of the 57 Ma (Devyatkin and Smelov, 1980) KS locality overlaps the cones of the reference poles for this age (Figure 11). The poles show a deviation of the longitude which is probably caused by the few constraints we have on possible bedding tilt.

Implications for regional tectonics

The average declination found in the area of 12.3° ±2.3° is undistinguishable from 13.6° ±2.4°, 11.0° ±8.9° and 14.9° ±3.4° predicted by the reference paths of BC02, SC05 and TO06 respectively. Schlupp (1996) suggested a specific tectonic setting to accommodate N-S shortening in western Mongolia. This model indicates clock-

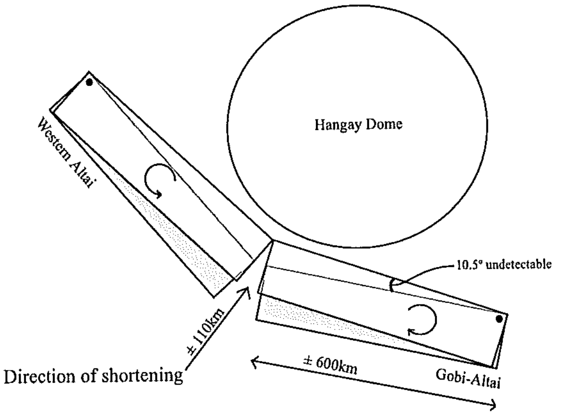

Figure 14: Schematic representation of the Schlupp (1996) rotation model to accomodate shortening in the Mongolian altai. This geometry shows that with the accuracy of the data, a shortening up to a maximum of 100km could be undetectable.

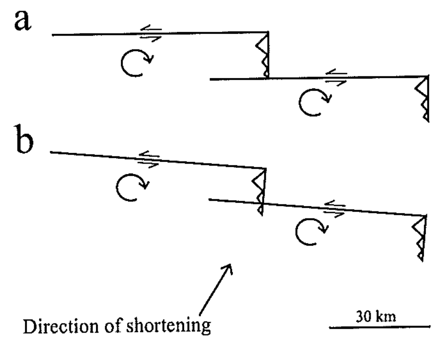

Figure 15: Cartoon to illustrate the areas of transpressional strike-slip and thrusting in a mechanism for the Gobi-Altai as proposed by Bayasgalan (1999), showing (a) before rotation and (b) after rotation. The scale is indicative.

wise rotation in the Gobi-Altai in a left-lateral fault system (Figure 1). Taking the Gobi-Altai to be rotating in a clockwise sense as a discrete block of ±600 km long, we calculated the amount of shortening that can be present and undetectable within the error margins of our data (Figure 14). For this experiment we used the reference declination of Schettino and Scotese (2005) because it allows the biggest, undetectable rotation. If we calculate the Δ declination with SC05 we come up with 1.3±9.2° which means we have a maximum of 10.5° of undetectable, clockwise rotation. A rotation like this would result in ±110 km of shortening southwest of the Hangay Dome. To create the topography of the Gobi-Altai this amount of shortening would largely be enough. We cannot prove nor disprove this model with our result.

To create the restraining bends, Bayasgalan (1999) suggested a model involving vertical axis rotations of rigid slats (Figure 15). The end of the oblique strike slip faults is marked by thrust faults (Figure 3). The amount of thrusting decreases with increasing distance from the strike-slip fault which implies a rotation of the thrusting unit, in this case a clockwise rotation (Figure 15). The units affected by strike-slip and thrusting should show changes in rotation with respect to the rigid unit/footwall. This postulated change in rotation of a few degrees lies well outside the accuracy limits of our paleomagnetic analysis. Comparing rotations of localities on both sides of the strike-slip faults did not reveal significant difference in rotation.

The concept of discrete slat rotation would cause initial strike-slip faults to rotate into orientations favourable for thrust displacements and restraining bend development. Newly developed strike-slip faults connect the original segments creating step-wise, en echelon strike-slip and thrust faults. The rotation associated with this kind of deformation can be inferred from the current geometry assuming that the direction of pure strike-slip did not change. This is the angle between the strike-slip and the oblique faults which in our case is ca 30° (Figure 3). Our results constrain this rotation to a maximum of 10.5°. Accordingly we exclude this rotational model for the northeastern Gobi-Altai.

The absence of significant local rotations means our data support the 'reactivaton' model. The direction of maximum stress makes an angle with the Paleozoic basement grain of the Gobi-Altai. Strike-slip faults develop in a segmented manner and their interconnection is by reactivation of former structures parallel to the basement grain, accommodating shortening. This may include the inversion of Mesozoic normal faults.

Inclination shallowing

The accretion of microplates and terranes to form Central Asian continent finished in pre-Cretaceous times and our Cretaceous data show that there has been no resolvable relative movement between central Asia and Europe since. Looking at the Cenozoic data, it is interesting to see if they confirm the rigid behaviour of central Asia with respect to the European Continent. Previous studies indicate that when comparing Cretaceous with Cenozoic data there is a "shallow inclination problem" (e.g. Westphal, 1993 and Chauvin et al., 1996). Cenozoic Paleomagnetic data systematically show inclinations that are shallower than inclinations calculated from the reference APWP, the amount of inclination shallowing ranging 15-30°. Supposed mechanisms explaining the contradiction are non-rigid behaviour of the Eurasian plate, syn- or post-depositional flattening, badly constrained reference path, non-dipolar geomagnetic field geometry and tectonic shortening (Westphal, 1993; Chauvin et al., 1996; Cogne et al., 1999; Tan et al., 2003).

In most studies, the inclination shallowing is found in red bed sedimentary rocks and explained in terms of a depositional or compaction-induced shallowing (Tan et al., 2003; Dupont-Nivet et al., 2004; Yan et al., 2005; Narumoto et al., 2006). To test whether the discrepancy in the data is real, one should compare results from the red bed sediments with volcanic deposits since the last are not affected by shallowing processes. This has been done several times for Cretaceous to Cenozoic deposits (Otofuji et al., 1995; Bazhenov and Mikolaichuk, 2002; Gilder et al., 2003). They show an inclination shallowing in red beds, but paleolatitudes of volcanic rocks coincide well with the latitudes predicted by the reference APWP. This implies that the shallowing is caused by syn- or post-sedimentary processes like compaction or initial shallow detrital remanent magnetisation.

Our Cretaceous data show good agreement with the synthetic reference poles obtained from Besse and Courtillot (2002). Our Cenozoic poles show a small but discernible offset with respect to the reference poles. We see that the inclinations of 30 Ma and 57 Ma are 10.0°±7.6 and 10.7°±13.0 less, respectivily, when compared with the inclinations predicted by the reference path of Besse and Courtillot (2002). This indicates the presence of a shallow inclination during Paleogene times which cannot be explained by syn- or post-sedimentary processes since the data come from volcanic rocks. The discrepancy can be caused by a primary dip during rock formation (for the plateaux) or a "missing" tectonic correction (for Khatan Suudal). Alternatively, our results could support the hypothesis of a non-dipolar geomagnetic field geometry during Cenozoic times (Westphal, 1993; Chauvin et al., 1996; Van der Voo and Torsvik, 2001). The shallowing (±10°) is less than most studies that include red beds (15°-30°, Cogné et al., 1999) and is probably partially caused by red beds compaction-induced shallowing.

Acknowledgements

I would like to thank dr. Douwe J.J. van Hinsbergen for continuous support and I thank G.C. Miolnir for providing the netwok making this collaboration possible. I would like to thank Prof. dr. C.G. Langereis for his support and I thank our Mongolian team-members for their assistance during the fieldwork. Finally I thank dr. W. Dickson Cunningham for support and for reviewing an earlier version of this manuscript. This research was supported by grants of the *Molengraaff Fonds* and the *K.F. Hein Fonds*.

References

Badarch, G., Cunningham, W.D., and Windley, B.F., 2002, A new terrane subdivision for Mongolia: implications for the Phanerozoic crustal growth of Central Asia: Journal of Asian Earth Sciences, v. 21, p. 87-110.

Baljinnyam, I., Bayasgalan, A., Borisov, B.A., Cisternas, A., Dem'yanovich, M.G., Ganbaatar, L., Kochetkov, V.M., Kurushin, R.A., Molnar, P., Philip, H., and Vashchilov, Y.Y., 1993, Ruptures of major earthquakes and active deformation in Mongolia and its surroundings: Geological Society of America Memoirs, v. 181.

Barry, T.L., 1999, Origins of Cenozoic basalts in Mongolia; a chemical and isotope study: Leicester, University of Leicester.

Bayasgalan, A., and Jackson, J., 1999, Field examples of strike-slip fault terminations in Mongolia and their tectonic significance: Tectonics, v. 18, p. 394-411.

Bazhenov, M.L., and Mikolaichuk, A.V., 2002, Paleomagnetism of Paleogene basalts from the Tien Shan, Kyrgyzstan: rigid Eurasia and dipole geomagentic field: EPSL, v. 195, p. 155-166.

Berkey, C.P., and Morris, K.K., 1927, Geology of Mongolia: New York, American Museum of Natural History, 475 pp. p.

Besse, J., and Courtillot, V., 2002, Apparent and True polar wander and the geometry of the geomagnetic field over the last 200 Myr: Journal of Geophyisical Research, v. 107, p. 2300.

Chauvin, A., Perroud, H., and Bazhenov, M.L., 1996, Anomalous low palaeomagnetic inclinations from Oligocen-Lower Miocene red beds of the south-west Tien Shan, Central Asia: Geophys. J. Int., v. 126, p. 303-313.

Cogne, J.-P., Halim, N., Chen, Y., and Courtillot, V., 1999, Resolving the problem of shallow magnetizations of Tertiary age in Asia: insights from paleomagnetic data from th Qiangtang, Kunlun, and Qaidam blocks (Tibet, China), and a new hypothesis: Journal of Geophyisical Research, v. 104, p. 17,715-17,734.

Cogné, J.-P., Halim, N., Chen, Y., and Courtillot, V., 1999, Resolving the problem of shallow magnetizations of Tertiary age in Asia: insights from paleomagnetic data from th Qiangtang, Kunlun, and Qaidam blocks (Tibet, China), and a new hypothesis: Journal of Geophyisical Research, v. 104, p. 17,715-17,734.

Cogne, J.-P., Kravchinsky, V., Halim, N., and Hankard, F., 2005, Late Jurassic-Early Cretaceous closure of the Mongol_okhotsk Ocean demonstrated by new Mesozoic palaeomagnetic results from the Trans-Baikal area (SE Siberia): Geophys. J. Int., v. 163, p. 813-832.

Cogné, J.-P., Kravchinsky, V., Halim, N., and Hankard, F., 2005, Late Jurassic-Early Cretaceous closure of the Mongol_okhotsk Ocean demonstrated by new Mesozoic palaeomagnetic results from the Trans-Baikal area (SE Siberia): Geophys. J. Int., v. 163, p. 813-832.

Collot, J.Y., Delteil, J., Lewis, K.B., Davy, B., Lamarche, G., Audru, J.C., Barnes, P., Chanier, F., Chaumillon, E., Lallemand, S., Mercier de Lepinay, B., Orpin, A., Pelletier, B., Sosson, M., Toussaint, B., and Uruski, C., 1996, From Oblique Subduction to Intra-Continental Transpression: Structures of the Southern Kermadec-Hikurangi Margin from Multibeam Bathymetry, Side-Scan Sonar and Seismic Reflection: Marine Geophysical Researches, v. 18, p. 357-381.

Cunningham, W.D., 1998, Lithospheric controls on late Cenozoic construction of the Mongolian Altai: Tectonics, v. 17, p. 891-902.

Cunningham, W.D., 2005, Active intracontinental transpressional mountain building in the Mongolian Altai: Defining a new class of orogen: EPSL, v. 240, p. 436-444.

Cunningham, W.D., Windley, B.F., Dorjnamjaa, D., Badamgarov, J., and Saandar, M., 1996, Late Cenozoic transpression in southwestern Mongolia and the Gobi Altai-Tien Shan connection: EPSL, v. 140, p. 67-82.

Cunningham, W.D., Windley, B.F., Owen, L.A., Barry, T., Dornjnamjaa, D., and Badamgarav, J., 1997, Geometry and style of partitioned deformation within a late Cenozoic transpressional zone in the eastern Gobi Altai Mountains, Mongolia: Tectonophysics, v. 277, p. 285-306.

Day, R., Fuller, M., and Schmidt, V.A., 1977, Hysteresis properties of titanomagnetites: grain-size and compositional dependence: Physics of the Earth and Planetary Interiors, v. 13, p. 260-267.

Devyatkin, Y.V., and Smelov, S.B., 1980, Position of basalts in the Cenozoic sedimentary sequence of Mongolia: International Geology Review, v. 22, p. 307-317.

Dunlop, D.J., 2002, Theory and application of the Day plot (Mrs/Ms versus Hcr/Hc) 1. Theoretical curves and tests using titanomagnetite data: Journal of Geophyisical Research, v. 107, p. EPM 4.

Dupont-Nivet, G., Robinson, D., Butler, R.F., Yin, A., and Melosh, H.J., 2004, Concentration of crustal displacement along a weak Altyn Tagh fault: Evidence from paleomagnetism of the northern Tibetan Plateau: Tectonics, v. 23, p. TC1020, doi:10.1029/2002TC001397.

Enkin, R.J., Yang, Z., Chen, Y., and Courtillot, V., 1992, Paleomagnetic Constraints on the Geodynamic History of the Major Blocks of China From the Permian to the Present: Journal of Geophyisical Research, v. 97, p. 13953-13989.

Garfunkel, Z., 1988, Regional Deformation by Block Translation and Rotation: In: Kissel, C., Laj, C. (Eds.), Paleomagnetic Rotations and Continental Deformation. Nato ASO Ser. 254, p. 181-208.

Gilder, S., Chen, Y., Cogne, J.-P., Tan, X., Courtillot, V., Sun, S., and Li, Y., 2003, Paleomagnetism of Upper Jurassic to Lower Cretaceous volcanic and sedimentary rocks from the western Tarim Basin and implications for inclination shallowing and absolute dating of the M-0 (ISEA?) chron: EPSL, v. 206, p. 587-600.

Hallimond, A.F., and Herroun, E.F., 1933, Laboratory determinations of the magnetic properties of certain igneous rocks: Proc. Roy. Soc., v. 141, p. 302-314.

Hankard, F., Cogné, J.-P., and Kravchinsky, V., 2005, A new Late Cretaceous paleomagnetic pole for the west of Amuria block (Khurmen Uul, Mongolia): EPSL.

Hankard, F., Cogné, J.-P., Quidelleur, X., Lkhagvadorj, P., and Bayasgalan, A., 2006, Paleomagnetism and K-Ar dating of Cretaceous basalts from Mongolia: Geophys. J. Int., v. submitted!

Helo, C., Hegner, E., Kröner, A., Badarch, G., Tomurtogoo, O., Windley, B.F., and Dulski, P., 2006, Geochemical signature of Paleozoic accretionary complexes of the Central Asian Orogenic Belt in South Mongolia: Constraints on arc environments and crustal growth: Chemical Geology, v. 227, p. 236-257.

Howard, J.P., Cunningham, W.D., and Davies, S.J., 2006, Competing processes of clastic deposition and compartmentalized inversion in an actively evolving transpressional basin, western Mongolia: Journal of the Geological Society, v. 163, p. 657-670.

Howard, J.P., Cunningham, W.D., Davies, S.J., Dijkstra, A.H., and Badarch, G., 2003, The stratigraphic and structural evolution of the Dzereg Basin, western Mongolia: clkastic sedimentation, transpressional faulting and basin destruction in an intraplate, intracontinental setting: Basin Res., v. 15, p. 45-72.

Johnson, C.L., Webb, L.E., Graham, S.A., Hendrix, M.S., and Badarch, G., 2001, Sedimentary and structural records of late Mesozoic high-strain extension and strain partitioning, East Gobi basin, southern Mongolia: Geological Society of America Memoir, v. 194, p. 413-433.

Kirschvink, J.L., 1980, The least-squares line and plane and the analysis of palaeomagnetic data.: Geophysical Journal of the Royal Astrological Society, v. 62, p. 699-718.

McFadden, P.L., 1990, A new fold-test for palaeomagnetic studies: Geophys. J. Int., v. 103, p. 163-169.
McFadden, P.L., and Lowes, F.J., 1981, The discrimination of mean directions drawn from Fisher distributions: Geophys. J. Roy. Astron. Soc., v. 67, p. 19-33.
McFadden, P.L., and McElhinny, M.W., 1988, The combined analysis of regamnetisation circles and direct observations in paleomagnetism: Earth Planet. Sci. Lett., v. 87, p. 161-172.
McFadden, P.L., and McElhinny, M.W., 1990, Classification of the Reversal Test in Paleomagnetism: Geophys. J. Int., v. 103, p. 725-729.
McFadden, P.L., Merrill, R.T., McElhinny, M.W., and Lee, S., 1991, Reversals of the Earth's Magnetic Field and Temporal Variations of the Dynamo Families: Journal of Geophyisical Research, v. 96, p. 3923-3933.
Mullender, T.A.T., Van Velzen, A.J., and Dekkers, M.J., 1993, Continuous drift correction and separate identification of ferrimagnetic and paramagnetic contribution in thermamagnetic runs: Geophys. J. Int., v. 114.
Narumoto, K., Yang, Z.Y., Takemoto, K., Zaman, H., Morinaga, H., and Otofuji, Y., 2006, Anomalously shallow inclination in middle-northern part of the South China block: palaeomagnetic study of Late Cretaceous red beds from Yichang area: Geophys. J. Int., v. 164, p. 293-300.
Nur, a., Ron, H., and Scotti, O., 1988, Mechanics of distributed fault and block rotation: In: Kissel, C., Laj, C. (Eds.), Paleomagnetic Rotations and Continental Deformation. Nato ASO Ser. 254, p. 209-228.
Otofuji, y., Itaya, T., Wang, H.C., and Nohda, S., 1995, Palaeomagnetism and K-Ar dating of Pleistocene colcanic rocks along the Altyn Tagh Fault, northern border of Tibet: Geophys. J. Int., v. 120, p. 367-374.
Pruner, P., 1992, Palaeomagnetism and palaeogeography of Mongolia from the Carboniferous to the Cretaceous-final report: Physics of the Earth and Planetary Interiors, v. 70, p. 169-177.
Roberts, A.P., Pike, C.R., and Verosub, K.L., 2000, First-order reversal curve diagrams: A new tool for characterizing the magnetic properties of natural samples: Journal of Geophyisical Research, v. 105, p. 28461-28475.
Schettino, A., and Scotese, C.R., 2005, Apparent polar wander paths for the major continents (200 Ma to the present day): a palaeomagnetic reference frame for global plate tectonic reconstructions: Geophys. J. Int., v. 163, p. 727-759.
Schlupp, A., 1996, Néotectonique de la Mongolie occidentale analysée a partir de données de terrain, sismologiques et satellitaires: Strasbourg, Université Louis Pastuer.
Sengör, A.M.C., Natal'in, B.A., and Burtman, V.S., 1993, Evolution of the Altaid tectonic collage and Palaeozoic crustal growth in Eurasia: Nature, v. 364, p. 299-306.
Strik, G., 2004, Palaeomagnetism of late Archaean flood basalt terrains: implications for early Earth geodynamics and geomagnetism: Utrecht, Utrecht University.
Tan, X., Kodama, K.P., Chen, H., Fang, D., Sun, D., and Li, Y., 2003, Paleomagnetism and magnetic anisotropy of Cretaceous red beds from the Tarim basin, northwest China: Evidence for a rock magnetic cause of anomalously shalow paleomagnetic inclinations from central Asia: Journal of Geophyisical Research, v. 108.
Tapponnier, P., and Molnar, P., 1979, Active faultring and cenozoic tectonics of the Tien Shan, Mongolia, and Baykal regions: J. Geophys. Res., v. 84, p. 3425-3459.
Tauxe, L., and Watson, G.S., 1994, The foldtest: an eigen analysis approach: EPSL, v. 122, p. 331-341.

Taylor, G.K., Grocott, J., Pope, A., and Randall, D.E., 1998, Mesozoic fault systems, deformation and fault block rotation in the Andean forearc: a crustal scale strike-slip duplex in the Coastal Cordillera of northern Chile: Tectonophysics, v. 299, p. 93-109.
Torsvik, T.H., Dietmar Müller, R., Van der Voo, R., Steinberger, B., and Gaina, C., 2006, Global Plate Motion Frames: Toward a Unified Model: submitted.
Traynor, J.J., and Sladen, C., 1995, Tectonic and stratigraphis evolution of the Mongolian People's Republic and its influence on hydrocarbon geology and potential: Marine and Petroleum Geology, v. 12, p. 35-52.
Van der Voo, R., 1990, The reliability of paleomagnetic data: Tectonophysics, v. 184, p. 1-9.
Van der Voo, R., Spakman, W., and Bijwaard, H., 1999, Mesozoic subducted slabs under Siberia: Nature, v. 397, p. 246-249.
Van der Voo, R., and Torsvik, T.H., 2001, Evidence for late Paleozoic an Mesozoic non-dipole fields provides an explanation for the Pangea reconstruction problems: Earth Planet. Sci. Lett., v. 187, p. 71-81.
Vandamme, D., 1994, A new method to determine paleosecular variation: Physics of the Earth and Planetary Interiors, v. 85, p. 131-142.
Vassallo, R., Jolivet, M., Ritz, J.F., Braucher, R., Larroque, C., Sue, C., Todbileg, M., and Javkhlanbold, D., 2006, Uplift age and rates of the Gurvan Bogd system (Gobi-Altay) by apatite fission track analysis: EPSL, v. in revision.
Vassallo, R., Ritz, J.F., Braucher, R., and Carretier, S., 2005, Dating faulted alluvial fans with cosmogenic 10Be in the Gurvan Bogd mountain range (gobi-Altay, Mongolia): climatic and tectonic implications: Terra Nova, v. 17, p. 278-285.
Vernant, P., Nilforoushan, F., Hatzfeld, D., Abbassi, M.R., Vigny, C., Masson, F., Nankali, H., Martinod, J., Ashtiani, A., Bayer, R., Tavakoli, F., and Chéry, J., 2004, Present-day crustal deformation and plate kinematics in the Middle East constrained by GPS measurements in Iran and northern Oman: Geophys. J. Int., v. 157, p. 381-398.
Wesnousky, S.G., 2005, The San Andreas and Walker Lane fault systems, western North America: transpression, transtension, cumulative slip and the structural evolution of a major transform plate boundary: Journal of Structural Geology, v. 2005, p. 1505-1512.
Westphal, M., 1993, Did a large departure from the geocentric axial dipole hypothesis occur during the Eocene? Evidence from the magnetic polar wander path of Eurasia: EPSL, v. 117, p. 15-28.
Yan, M.D., Van der Voo, R., Tauxe, L., Fang, X.M., and Pares, J.M., 2005, Shallow bias in Neogene palaeomagnetic directions from the Guide basin, NE Tibet, caused by inclination error: Geophys. J. Int., v. 163, p. 944-948.
Zhao, X., Coe, R.S., Zhou, Y., Wu, H., and Wang, J., 1990, New paleomagnetic results from northern China: collision and suturing with Siberia and Kazakhstan: Tectonophysics, v. 181, p. 43-81.
Zijderveld, J.D.A., 1967, A.C. demagnetization of rocks: analysis of results: In: D.W. Collinson, K.M. Creer, S.K. Runcorn (Eds.), Methods in Paleomagnetism, Elsevier, NewYork, p. pp. 245-286.
Zonenshain, L.P., Kuzmin, M.I., and Natapov, L.M., 1990, Geology of the USSR: A Plate Tectonic Synthesis, AGU, 240 p.